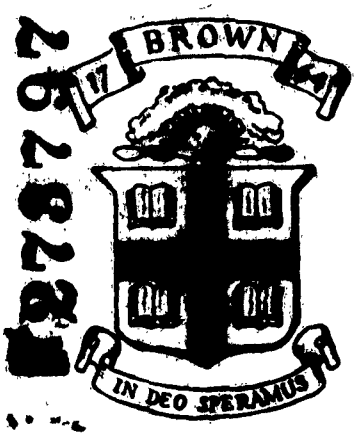

Division of Engineering
BROWN UNIVERSITY
PROVIDENCE, R. I.

AN INVESTIGATION OF THE ENERGY CRITERION IN SNAP BUCKLING PROBLEMS WITH APPLICATION TO CLAMPED ARCHES

BY

A. GJELSVIK and S.R BODNER

Department of the Navy
Office of Naval Research
Contract Nonr 562(20) NR-064-424
Technical Report No. 28

Nonr-562(20)/28

February 1962

Nonr-562(20)/28

AN INVESTIGATION OF THE ENERGY CRITERION IN SNAP BUCKLING PROBLEMS WITH APPLICATION TO CLAMPED ARCHES

by

A. Gjelsvik and S. R. Bodner

Technical Report No. 28
Division of Engineering
Brown University
Providence, Rhode Island

February 1962

Sponsored by
Department of the Navy
Office of Naval Research
Under Contract Nonr-562(20)
Task Order NR-064-424

Nonr-562(20)/28

AN INVESTIGATION OF THE ENERGY CRITERION IN SNAP BUCKLING PROBLEMS WITH APPLICATION TO CLAMPED ARCHES†

by

A. Gjelsvik* and S. R. Bodner**

ABSTRACT

A critical analysis is presented of the significance of the energy criterion for systems that exhibit snap buckling. The results of energetic analyses are compared to solutions of the differential equations for the nonlinear behavior of a clamped low arch subjected to a central concentrated load. The differential equation analyses include consideration of transitional non-symmetrical buckling modes. The snap buckling of low arches in the presence of high temperature creep is also considered. Experiments are described on the deformation of such arches under static and creep conditions.

---

† The results in this paper were obtained in the course of research sponsored by the Office of Naval Research under Contract Nonr-562(20) with Brown University.

* Research Assistant, Division of Engineering, Brown University.

** Associate Professor, Division of Engineering, Brown University.

Principal Symbols

a		central height of mechanical model; also non-dimensional amplitude of symmetrical deflection of arch
b		non-dimensional amplitude of anti-symmetrical deflection of arch
f		width of arch cross section
k		spring constant
t		thickness of arch
u,w		tangential and radial displacements at middle surface of arch
v		generalized displacement
A		cross sectional area; also deflection amplitude
B		deflection amplitude
E		Young's modulus
F		force in spring component of the model
H		total energy of system
H^*	$=$	$H\lambda/\beta^5$
P		applied load
P_e		energy load (same as "intermediate" or "dead weight" buckling load)
P_L		lower buckling load
P_U		upper buckling load
P^*	$=$	$PR/Et^2f\beta$
L		length of arms of model
R		radius of arch centerline
T		axial force in the arms of the model
α		angular coordinate for arch (measured from centerline)
β		half of angle subtended by arch

γ		imperfection amplitude
δ		deflection of midpoint of model
ε		strain
ξ	=	α/β
$\varkappa$		change of curvature of arch
λ	=	$\beta^2 R/t$
σ		stress

Introduction.

The fundamental cause of the large discrepancy between buckling values predicted by the classical eigenvalue theory and experimental results for spherical and cylindrical shells was shown by von Karman and Tsien, [1] [2], to be due to the existence of post buckling stable equilibrium states characterized by loads appreciably lower than the classical buckling load, e.g. Fig. 1. They advanced the hypothesis that somehow the shell could jump to these equilibrium states at loads less than the linear buckling load so that the lowest load for such states, point 2 of Fig. 1, should be considered the minimum load at which buckling was possible. The question was left open as to how the transition from the initial state to the buckled state was to take place since, unlike classical buckling theory, these are not geometrically adjacent states. They postulated, however, that the transition may be connected with geometrical imperfections, small dynamic disturbances or possibly with unsymmetrical deformations not included in the analyses [3]. The values von Karman and Tsien obtained for the lower buckling loads in [1] and [2] were in surprisingly good agreement with available experimental results.

A weakness in the lower buckling load as a realistic buckling criterion was pointed out by Friedrichs [4]. He showed that at the lower buckling load the system of the shell and the loading is at a higher energy level in the buckled than in the unbuckled state. Since no energy is transferred to the system during the jump, but some may be lost, it can only be expected to jump from a state of a higher to a state of lower energy level. If no energy is lost

the minimum load at which a jump can take place is then the load at which the total energy in the buckled and unbuckled states are equal. Friedrichs called this the intermediate buckling load. He did not try to explain why or how the jump could take place. Friedrichs also analyzed the stability of the complete sphere using a boundary layer treatment and relaxed some unnecessarily restrictive assumptions employed by von Karman and Tsien. Friedrichs found that both the minimum and the intermediate buckling loads were zero in the boundary layer development for a complete sphere.

Tsien [5,6] attempted to explain the mechanism of snap buckling by introducing additional energy considerations. His energy criterion stated that under average laboratory or actual service conditions the most probably equilibrium state is that with the lowest possible energy level. In calculating the energy levels before and after buckling the elasticity of the loading system must be taken into account. Different buckling loads are therefore predicted for the same shell with different loading systems by this theory. For dead loading the load necessary to cause instability is the same as Friedrich's intermediate buckling load. Tsien's principle, however, adds the assumption that there always are disturbances of sufficient magnitude present to overcome the stability of the unbuckled state. However, if disturbances of such a magnitude are admitted there appears to be no reason why the system could not jump from a state of lower to a state of higher energy, provided a stable buckled state exists at that load. The lower buckling load is the lowest load for which a stable buckled state exists, and therefore the lowest load for which the system could

remain in a buckled position if sufficiently disturbed. Below this load only oscillations about the unbuckled state can take place. The energy load, as defined in this manner, therefore loses its original meaning.

Tsien investigated the stability of complete spheres under hydrostatic pressure and cylindrical shells under axial compression, and obtained fairly good agreement with experimental results. Although Tsien's results and more recent work using the energy criterion by Lo, Crate and Schwarz [7] gave good agreement with experiments, there are strong objections to its validity and therefore to its acceptability. These objections are well summarized in the survey paper by Fung and Sechler [8] and are based on the fuzziness of the theoretical foundation of the energy criterion and especially the fact that it requires a knowledge of the geometrically removed post buckling state to determine the onset of buckling. In addition, the tests of Kaplan and Fung on shells [9] showed little difference for different loading conditions in opposition to the theory. Tests on simply supported shallow arches [10] also agreed well with the upper buckling load values which were appreciably different from the loads predicted by the energy criterion.

At the present time the trend is away from intuitive approaches such as the energy criterion and attempts are made to solve the governing differential equations by the use of high speed digital computers, e.g. Keller and Reiss [11], Budiansky [12] and Thurston [13]. There is little doubt that this approach will eventually give most of the required answers since for completely static loading the buckling load must be a peak point of the appropriate load

deflection curve. Such curves are, however, extremely difficult to obtain since they should incorporate initial deflections of the shell, the appropriate stresses and deformations that exist in the pre-buckling state and, above all, must include the correct mode into which the shell would initially buckle. Aside from the basic problems associated with handling nonlinear problems, additional complications arise when the important initial deflections are not necessarily those having the form of the buckled shape,and when transitional buckling modes appear that may also be appreciably different from both the initial and the final shapes. The formulation and numerical solution of nonlinear problems of this generality still presents formidable obstacles.

Because of the difficulties mentioned above in contrast to the simplicities offered by an energy approach, the authors have felt it worthwhile to reexamine the theoretical basis of the energy criterion. Its relative simplicity makes it particularly attractive for problems in which additional complicating features such as anisotropy, inhomogeneity, and combined loadings appear. In the following discussion the term "energy load" or "energy criterion" will be restricted to mean Friedrich's intermediate load or, alternatively, Tsien's "dead weight" energy load.

The first part of this paper is devoted to an analysis of the significance of the energy load for systems having force deflection characteristics of the form shown in Fig. 1. The general discussion is preceded by a complete analysis of a simple mechanical model which has such a load deflection curve. The discussion itself is completely general and is not restricted to arch and shell

structures - the arguments may be relevant to other systems which experience similar behavior.

The second part of this paper is devoted to comparing the results of the energy approach with those of more thorough theoretical analyses of low arches. A subsequent paper will investigate the energy criterion in relation to the behavior of clamped spherical caps and complete spherical shells.

A fairly complete theoretical and experimental analysis of clamped shallow arches is performed. The theoretical work includes consideration of a number of symmetrical deflection modes as well as transitional non-symmetrical buckling. The experiments on arches produced buckling load values and complete load deflection curves which included the unstable transition region. The agreement between theory and experiment was fairly good.

The energy load computed on the basis of ideal geometry and axially symmetrical buckling is shown to be a lower bound for snap buckling for systems influenced by non-symmetrical transitional buckling modes. For a particular class of systems, the energy load is also found to be unaffected by certain forms of initial imperfections and to be a lower bound for snap buckling in the presence of those imperfections. The systems and imperfections are restricted to those for which the load deflection curve with and without the inclusion of imperfections is anti-symmetrical about a common straight line through the origin. Although only few structural systems fall into this class, e.g., clamped arches, the actual behavior of spherical caps and presumably other systems is close to being the same. The energy load is found to be relatively

insensitive to arbitrarily chosen buckling modes. In addition, both the theoretical and experimental results for arches and spherical caps show that the difference between the energy load and the upper buckling load diminishes the more the system is influenced by non-symmetrical transitional modes and by destabilizing initial imperfections.

Model for Snap Buckling.

To gain a better understanding of some of the concepts mentioned in the introduction, as well as to introduce some new ones, a simple mechanical model will first be investigated. The bar spring system shown in Fig. 2 has many important features in common with a low arch and a shallow cap. The model is considered as hinged in the middle and at the ends, and subjected to a single load P at the apex. The discussion will be limited to a low frame, that is one for which

$$(a/L) << 1 \tag{1}$$

where a is the unstrained height and 2L is the width of the frame. From the geometry the equilibrium equation is immediately obtained:

$$P = k\delta + 2T(a-\delta)/L \tag{2}$$

where δ is the vertical displacement of the apex, k the spring stiffness and T the compressive force in the arms. Also from geometry the strain in the arms is

$$\varepsilon = \delta(\delta-2a)/2L^2 \tag{3}$$

From Hook's law the force in the arms is therefore

$$T = -(AE/2L^2)\delta(\delta - 2a) \tag{4}$$

where AE is the stiffness of the arms. Substituting for T in the equilibrium equation (2) yields the load deflection relation of the model

$$P = k\delta + (AE/L^3)\delta(\delta-a)\ (\delta-2a) \tag{5}$$

This is plotted in Fig. 3.

The curve can be considered as composed of two parts, a straight line caused by the spring stiffness k, and a curve anti-symmetrical about $\delta = a$. According to the classical criterion instability occurs when the first maximum is reached or at the point A in Fig. 3. This is usually called a limit or critical point. In contrast to most buckling problems instability is not caused by a bifurcation of the equilibrium state but by the load reaching a maximum. The lower buckling load of von Karman and Tsien would correspond to the minimum point or point B in Fig. 3. Both these points are obtained by setting

$$\frac{dP}{d\delta} = 0 \tag{6}$$

By substitution from (5), this yields

$$\delta = a \pm [a^2/3 - (kL^3/3AE)]^{\frac{1}{2}} \tag{7}$$

The plus sign is clearly associated with the lower buckling load and the negative with the limit point or the upper buckling load. These two loads will coincide in a point of inflection with a

horizontal tangent at $\delta = a$ when the quantity under the root is zero. If the root is imaginary the load deflection curve will be continually rising and always stable. For instability to be possible therefore

$$(a^2AE/kL^3) \geq 1 \tag{8}$$

The intermediate buckling load or the energy load as defined by Friedrichs, or by Tsien for a dead load, can be determined most easily from the geometry of the load deflection curve. At the energy load the total energy in the buckled and unbuckled states are equal, or the change in energy from one to the other is zero. In Fig. 4 the decrease in potential energy of the load in going from the unbuckled to the buckled state is given by the rectangle ABCD. The increase in strain energy of the spring and the arms is given by the area under the load deflection curve between B and C. The change in total energy will then be given by the difference between these two areas. At the energy load, the two areas must be equal. From the symmetry of the curve it is seen that this occurs when the line BC passes through the crossing point of the straight line due to the spring and the curve due to the effect of the arms. The energy load is therefore

$$P_e = ka \tag{9}$$

This is a function of the spring stiffness and the geometry but is independent of the properties of the arms. This is quite remarkable and shows that imperfections thathave the effect of reducing the stiffness of the arms only will leave the energy load unchanged.

The energy load will cease to exist when the curve is reduced to one with a point of inflection with a horizontal tangent. The upper, lower and energy load would then be equal. If imperfections of the arms are sufficiently large, the energy load may cease to exist, but in that case instability would not occur either. Consideration of imperfections of the arms only would result in the energy load being a lower bound on the loads that can cause instability. This is true regardless of the magnitude of the imperfections. It may be objected that the height "a" of the model enters into the expression for the energy load. Variations in "a" however, should not be considered to be imperfections in the usual sense of buckling problems but as changes in overall geometry. The same could be said about the length of a strut in ordinary Euler buckling, i.e. imperfections are considered to be deviations from straightness and not changes in the length. In the general class of nonlinear problems under consideration, however, more attention must be given to the definition of geometric "imperfections".

As an example of an imperfection, the arms can be considered to have a sinusoidal centerline with amplitude α . The shortening e of one of the arms subjected to the compressive force T is then:

$$e = \frac{\gamma^2}{4}\left[\frac{T}{T-(\pi^2 EI/L^2)}\right]^2 \frac{\pi^2}{L} + \frac{TL}{AE} \qquad (10)$$

This must be equal to the shortening of the arms as caused by the lowering of the apex of the model.

Then from Eq. (3),

$$\frac{\delta}{2L}(2a-\delta) = \frac{\gamma^2}{4}\left[\frac{T}{T-(\pi^2EI/L^2)}\right]^2 \frac{\pi^2}{L} + \frac{TL}{AE} \qquad (11)$$

From the equilibrium equation (2) the value of T can be substituted to give the load deflection curve

$$\frac{\gamma^2\pi^2}{4L}\left[\frac{(P-k\delta)/(a-\delta)}{[(P-k\delta)/(a-\delta)]-2\pi^2EI/L^3}\right]^2 + \frac{(P-k\delta)L^2}{2AE(a-\delta)} - \frac{\delta(2a-\delta)}{2L} = 0 \qquad (12)$$

This is plotted in Fig. 5 for different values of γ. It can be seen that the upper buckling load is reduced by γ increasing whereas the energy load remains unchanged.

If the possibility of the arms buckling is admitted a different mode of instability is added. Let

$$T_E = \pi^2EI/L^2 \qquad (13)$$

be the Euler load of the arms. For

$$T < T_E$$

the load deflection curve is still given by (5), but when $T = T_E$ it is given by substituting for T from (13) in the equilibrium equation (2). This yields

$$P = k\delta + (2\pi^2EI/L^3)\ (a-\delta) \qquad (14)$$

which is a straight line passing through $P = ka$ and $\delta = a$ as shown in Fig. 6. Instability will now occur when the force in the arms becomes T_E or at the point B in the figure provided the slope of the line BC is negative or zero. If the slope is positive the load deflection curve will be continually rising and stable for

all loads. From Fig. 6 it is seen that the slope becomes positive when the column buckling load P_T is less than the energy load P_e. The energy load is therefore again the dividing point between stability and instability if the possibility of transitional buckling modes is admitted. The energy load is therefore also in this sense a lower bound on the snap buckling load of the complete system.

From the discussion of the model it is seen that the energy load calculated on the basis of perfect geometry and the basic deformation mode is a lower bound on the snap-buckling load in the presence of imperfections or additional transitional modes. It is of interest to see if this interpretation of the energy load is true only for this particular model or if it is true for more general classes of systems.

Influence of Transitional Buckling and Imperfections in Systems That Exhibit Snap Buckling.

For systems having load deflection curves similar to Fig.1 in the absence of both transitional buckling modes and initial imperfections, the problem is to determine the changes those factors could have on the basic curve and the relevancy, if any, of the energy criterion. The nature of admissible load deflection curves for transitional buckling modes will first be examined. Transitional buckling refers to the case where the mode of the intermediate unstable equilibrium states is essentially different from both the initial state and the final buckled state. Examples of transitional buckling are column buckling of the model previously discussed and anti-symmetrical buckling of simply supported arches

which was investigated by Marguerre [14] and is discussed in [3].

The basic system under discussion will be assumed to have only one pair of stable initial and final equilibrium states in the load range $P_L \leq P \leq P_U$ as indicated by the curves OA and BC respectively in Fig. 7. Load deflection curves that cross over themselves will be ruled out. The overall (or average) behavior of most structural elements that exhibit snap buckling would have equilibrium characteristics similar to Fig. 7. The relevant question for transitional buckling is the nature of possible unstable equilibrium paths connecting the two stable branches. Alternatively, the problem is the determination of admissible paths connecting the two stable states that do not require any input or release of kinetic energy.

In discussing snap buckling of a system with many degrees of freedom it is necessary to introduce some characteristic displacement function in order to describe the geometric dependence. The function that appears to be an appropriate and consistent indicator of the gross behavior is the one that appears in the expression for the work done by the external force system (the generalized displacement). For the case of a concentrated force this would be the actual displacement at the point of application and in the direction of the applied force. For hydrostatic pressure it would be the change in volume. The integrated average displacement used as the geometric reference by Budiansky [12] is, to first order terms, equivalent to a volume change. The generalized displacement from the work expression will be used as the

geometric reference parameter in the following general discussions and in the particular examples.

The elastic strain energy U of the system is assumed to be completely defined in the unbuckled and buckled stable equilibrium states. The work done by the external force system P during a small change in the generalized displacement v is Pdv. In the absence of kinetic energy this must be equal to the change of strain energy during the same process,

$$dU = Pdv \tag{15}$$

If the total potential energy H defined as

$$H = U - Pv$$

is introduced, then

$$dH = dU - Pdv - vdP$$

and from (15)

$$dH = - vdP \tag{16}$$

From the definition of the total energy it is seen that it is also completely defined in the unbuckled and buckled stable equilibrium states. Integrating (16) along a path connecting two such states a and b gives

$$H_b - H_a = - \int_a^b vdP \tag{17}$$

where the integral depends upon the path. This integral can be interpretated graphically as the area between the path and the P axis. This area must therefore be the same for all paths between the states a and b if no kinetic energy is involved. At the energy load, P_e, in particular, $H_1 = H_2$, and setting a = 1, b = 2 to correspond to the points in Fig. 7,

$$\int_1^2 v dP = 0 \tag{18}$$

and the area is therefore zero. This is the same criterion that was used to determine the energy load for the model. Some equilibrium curves that would satisfy (18) are shown in Fig. 7 by the dashed lines. Portions of these curves, except the straight line, would be stable equilibrium states aside from OA and BC and must therefore be excluded. The straight horizontal line is therefore the only possible completely unstable or neutral equilibrium path connecting the unbuckled and buckled states at the energy load.

Starting from above the energy load, possible unstable equilibrium must be similar to the curve 3-4 in Fig. 7. Since the portion of the curve 1-3-5-4-2 can be considered as a path connecting 1 and 2 for which (18) holds, it follows that the area enclosed by 1-3-5 must be equal to (minus) the area enclosed by 5-4-2. The path 3-4 must also be monotonically decreasing to satisfy the condition that it be a locus of unstable or neutral equilibrium states. Starting from points below the energy load, no path satisfying the requirements can be found. The energy load is therefore the minimum load from which unstable equilibrium

paths could start, i.e. it is the minimum load for which a bifurcation of equilibrium due to the occurrence of other modes would lead to snap buckling of the system.

Some other general statements follow almost directly. For a system with a load deflection curve of the type shown in Fig. 1 the energy load must lie between the upper and lower buckling loads since the two shaded areas must be equal. The three critical loads are equal when the load deflection curve has a point of inflection with a horizontal slope. It is also seen that for the same load the total energy H along BC (Fig. 7) is less than H along OA for $P > P_e$. Since BC is the locus of stable equilibrium states, the potential energy in adjacent non-equilibrium states (at the same load) must be greater than for points on BC. The energy load P_e can therefore be defined as the minimum load for which the total potential energies are equal in the unbuckled state (along OA) and in any arbitrary buckled state whether or not it is an equilibrium state. The buckled state that gives the true minimum must, of course, be the equilibrium state 2. This variational formulation for calculating the energy load may be useful since it does not require the prior determination of the buckled equilibrium states BC. The energy load determined by such a variational procedure would be an upper bound if the initial state along OA is exact and the buckled state is approximated, and would be a lower bound on the real energy load if the reverse were true.

The role of imperfections in nonlinear systems is a much more difficult problem. Part of the difficulty is due to the vagueness of any definition of "imperfections" other than any

arbitrary deviation from the pre-assumed "ideal" geometry that satisfies the geometric boundary conditions. It is not surprising that "imperfections" can have vastly different effects according to their manner of introduction in a specific problem.

In linear buckling problems, imperfections are generally taken to mean the deviations from the idealized geometry that influence the destabilizing (or stabilizing) role of the membrane stresses. This same concept is usually used in nonlinear problems in the sense that the terms due to the imperfections appear only in expressions for the membrane energy or in conjunction with membrane stresses in the differential equations. The imperfections do, however, influence the complete problem since the membrane and bending stresses and the displacements are all coupled in a nonlinear problem.

The imperfections considered in the analysis of the model were deviations from straightness of the arms and therefore had the same mode as that corresponding to transitional buckling. The energy load was found to be unchanged and to be a lower bound for snap buckling in the presence of these imperfections. Another kind of imperfection in the model problem would be a change in the height of the apex which would correspond to a change in the basic geometry and therefore in the energy load. It is convenient to designate these two basically different types of imperfections as A and B respectively for reference in discussing more complicated systems.

The general conditions required for imperfections to be of type A are of particular interest since the energy criterion then

has a definite physical interpretation. We shall consider systems for which the resistance to deformation can be subdivided into "bending" and "membrane" contributions and where the membrane stresses are symmetrical in the stress - generalized displacement plane with respect to a particular displacement value. This characteristic is shown in Fig. 8 where the stress deflection relationships are assumed to be symmetrical about the vertical line A-A. The strain energy of the membrane stresses is a quadratic function of the stresses and would therefore have the general form shown in Fig. 9. It would also be symmetric about A-A. The membrane stress contribution to the load deflection curve would then be anti-symmetric about A-A, since that curve is obtained by differentiating the potential energy with respect to the generalized deflection v . In nonlinear structural systems the terms corresponding to the bending resistance are generally linear in the displacements. The complete load deflection curve would then have the same form as that for the model, Fig. 3.

If the inclusion of geometric imperfections into the problem only alters the magnitude of the membrane stresses but does not change the bending contribution or the basic symmetry, then the energy load must remain unchanged. A sufficient, and seemingly necessary, condition that the energy load remain unchanged in the presence of geometric imperfections is, therefore, that the membrane stresses for the perfect system are all symmetrical about a common generalized displacement value, and that the only effect of the imperfections considered is to change the magnitudes of those membrane stresses without altering the symmetry. A further consequence of

these conditions is that, as was shown in the case of the model, the energy load would also be a lower bound on snap buckling in the presence of the imperfections. The imperfections would then be of type A discussed previously.

It does not seem possible, however, to determine a priori whether a given structural system and arbitrarily chosen imperfection functions will behave in the above manner. In the subsequent analyses it is found that the behavior of the symmetrically loaded clamped arch does conform with the stated conditions. For the clamped arch anti-symmetrical imperfections are found to be of type A (the transitional buckling mode is also anti-symmetrical), while symmetrical imperfections are of type B. The clamped spherical cap, on the other hand, does not possess the required symmetry properties of the membrane stresses, so that it cannot admit imperfections strictly of the A type. The symmetrical imperfections considered by Budiansky in [12] for the cap appear to have properties similar to those of type B.

Cylindrical shells also do not appear to have the properties required for a class of imperfections to be strictly of type A. It is interesting to note, however, that the results of [15, 16] approximate the expected results for imperfections of type A. The upper buckling load for the largest imperfection parameter that shows snap buckling is reasonably close to the energy load of the perfect shell.

Although the energy criterion does not maintain any definite physical meaning in the presence of imperfections of type B, which can be related to changes in the overall geometry, it can

serve as a measure of the gross influence of these imperfections on the nonlinear behavior of the system. The change in the energy load due to those imperfections would be an indication of the sensitivity of the system to the geometry changes. This viewpoint is of some practical interest since the computation of the energy load is considerably simpler than the complete solution of the nonlinear differential equations. This would be particularly true in problems where the mode of sensitive imperfections of type B are essentially different from either the transitional or final buckled modes, e.g. axi-symmetrical imperfections in cylinder buckling problems.

Analysis of a Clamped Low Arch Subjected to a Central Concentrated Load

The clamped low arch was chosen as a specific structural system to examine the general results of the preceding section. Although the simply supported arch has been thoroughly investigated by Fung and Kaplan [10] and by Biezeno and Grammel [17], the clamped condition initially appeared to offer more basic complicating features. In nonlinear problems particularly, a change in the boundary conditions can often alter the complete nature of the problem. The anticipated difficulties did not, in fact, materialize in this instance. The problem of the clamped arch, however, besides being of some practical interest, does serve as a very good example to discuss the significance of the energy load in relation to the upper buckling load, geometric imperfections, transitional buckling modes, and varying degree of approximation of solutions. The clamped arch problem also contains a number of

similarities to that of the uniformly loaded spherical cap. The trend of results of the arch problem serves as a good indicator of the behavior of the latter more complicated structure.

From the experimental side it is possible to obtain better control with fully clamped end conditions. This is especially true at high temperatures where binding at the supports would be a problem,and an important part of the general program was the investigation of snap buckling due to high temperature creep. The elastic buckling experiments, which were performed at room temperature, were concerned with obtaining complete load deflection curves, including the unstable regions, for a wide range of arch geometries.

(a) General Formulation.

The circular clamped arch loaded with a single central concentrated load as shown in Fig. 10 is analyzed. With the usual assumption for thin curved beams, the axial strain ε is

$$\varepsilon = (1/R)\,(u_\alpha - w) + (1/2R^2)\,(w_\alpha)^2 \qquad (19)$$

and $\varkappa$,the change in curvature,is

$$\varkappa = (1/R^2)w_{\alpha\alpha} \qquad (20)$$

where u is the tangential and w the radial displacement function, R is the radius of the arch,and α is the polar angle measured from the center of the arch. Differentiation with respect to α is denoted by the subscript α .

The strain energy due to the axial deformations , nondimensionalized by division by the factor EtfR,is

$$U_m = (1/2) \int_{-\beta}^{\beta} \varepsilon^2 d\alpha \tag{21}$$

and that due to bending is

$$U_b = (t^2/24) \int_{-\beta}^{\beta} \varkappa^2 d\alpha \tag{22}$$

where t is the thickness and f the width of the beam, E is Young's modulus and β half the included angle of the arch. The change in potential energy of the load, in non-dimensional form, is given by

$$U_p = - [P/EtRf](w)_{\alpha=0} \tag{23}$$

where P is the concentrated central load. The total energy H is given by

$$H = U_m + U_b + U_p \tag{24}$$

The tangential displacement function u can be eliminated from the energy expression. The variation of the total energy H with respect to u must be zero for equilibrium. Since u only appears in U_m, the membrane strain energy, this yields immediately

$$\varepsilon_\alpha = 0$$

or

$$\varepsilon = C \tag{25}$$

where C is a constant. Substituting in (25) from the strain displacement relation (19) and rearranging

$$u_\alpha = w - (1/2R)\,(w_\alpha)^2 + CR$$

Integrating between $\alpha = \beta$ and $\alpha = -\beta$ gives

$$[u]_{-\beta}^{\beta} = \int_{-\beta}^{\beta} [w-(1/2R)(w_\alpha)^2]d\alpha + [CR\alpha]_{-\beta}^{\beta}$$

The boundary conditions on u are

$$u = 0 \text{ at } \alpha = \pm \beta \tag{26}$$

The left hand side is therefore zero. Solving the remainder for the constant C which, from (25) is equal to ε, yields

$$\varepsilon = -(1/2R\beta)\int_{-\beta}^{\beta} [w-(1/2R)(w_\alpha)^2]d\alpha \tag{27}$$

Substituting this value for into the energy expression (24), and for x from (20), gives the total energy H as a function of w only

$$H = \frac{1}{4\beta^2}\left\{\int_{-\beta}^{\beta}(w - \frac{1}{2R}\,w_\alpha^2)d\alpha\right\}^2 + \frac{t^2}{24}\int_{-\beta}^{\beta} w_{\alpha\alpha}^2\, d\alpha - \frac{P}{EHt}[w]_\alpha = 0 \tag{28}$$

where the brackets in $(w_\alpha)^2$ and $(w_{\alpha\alpha})^2$ are left out. In the following when this is done it will always mean that the differentiation is performed first.

(b) Approximate Solution

A first numerical approximation can now be obtained by assuming a function for w. Let

$$w = Aw_1(\xi) + B\,w_2(\xi) \tag{29}$$

where w_1 is a symmetric and w_2 an anti-symmetric function in ξ. ξ is the ratio α/β and A and B are the amplitude of the two deflected shapes. Substituting this value w in the energy expression gives

$$H = (1/4R^2\beta)[\beta AC_1 + \beta BC_2 - (1/2R\beta)\ (A^2C_3 + 2ABC_4 + B^2C_5)]^2$$

$$+ (t^2/24R^4\beta^3)\ (A^2C_6 + 2ABC_7 + B^2C_8) - (P/EtRf)\ (AC_9 + BC_{10}) \tag{30}$$

where the constants are given by the integrals

$$C_1 = \int_{-1}^{1} w_1 d\xi \qquad C_2 = \int_{-1}^{1} w_2 d\xi$$

$$C_3 = \int_{-1}^{1} w_1 \xi^2 d\xi \qquad C_4 = \int_{-1}^{1} w_1 \xi w_2 \xi d\xi$$

$$C_5 = \int_{-1}^{1} w_2 \xi^2 d\xi \qquad C_6 = \int_{-1}^{1} w_1 \xi^2 \xi d\xi \tag{31}$$

$$C_7 = \int_{-1}^{1} w_1 \xi \xi w_2 \xi \xi d\xi \qquad C_8 = \int_{-1}^{1} w_2 \xi^2 \xi\ d\xi$$

$$C_9 = [w_1]_{\xi = 0} \qquad C_{10} = [w_2]_{\xi = 0}$$

Introducing non-dimensional amplitudes

$$a = (A/R\beta^2) \qquad b = (B/R\beta^2) \tag{32}$$

and load

$$P^* = (PR/Et^2 f\beta) \tag{33}$$

and a geometric parameter

$$\lambda = (\beta^2 R/t) \tag{34}$$

the energy can be written as

$$H^* = H\lambda/\beta^5 = (\lambda/4)\,[aC_1 + bC_2 - (1/2)\,(a^2C_3 + 2abC_4 + b^2C_5)]^2$$

$$+ (1/24\lambda)\,(a^2C_6 + 2abC_7 + b^2C_8) - P^*(aC_9 + bC_{10}) \tag{35}$$

Because of the symmetry and anti-symmetry of w_1 and w_2 it can be seen immediately that

$$C_2 = C_4 = C_7 = C_{10} = 0$$

The energy H^* therefore reduces to

$$H^* = (\lambda/4)[aC_1 - (1/2)(a^2C_3 + b^2C_5)]^2 + (1/24\lambda)(a^2C_6 + b^2C_8) - P^*aC_9 \tag{36}$$

For equilibrium:

$$\frac{\partial H^*}{\partial a} = 0 \quad \frac{\partial H^*}{\partial b} = 0$$

From the above this yields

$$P^*C_9 = (\lambda/2)[aC_1 - (1/2)(a^2C_3 + b^2C_5)](C_1 - C_3a) + (1/12\lambda)(aC_6) \tag{37}$$

$$(bC_5\lambda/2)[aC_1 - (1/2)(a^2C_3 + b^2C_5)] - (1/12\lambda)bC_8 = 0 \tag{38}$$

The last equation has the solutions

$$b = 0 \tag{39}$$

$$b = (2/C_5)[aC_1 - (a^2C_3/2) - (C_8/6\lambda^2C_5)]^{\frac{1}{2}} \qquad (40)$$

If the quantity under the root is negative, the only real solution is b = 0. The deformation will then by symmetrical. The condition that a real solution for b exists other than b = 0 is therefore that

$$aC_1 - (a^2C_3/2) - (C_8/6\lambda^2C_5) \geq 0$$

Which, when solved for a, gives

$$a \geq (C_1/C_3) - [(C_1/C_3)^2 - (C_8/3C_3C_5\lambda^2)]^{\frac{1}{2}} \qquad (41)$$

$$a \leq (C_1/C_3) + [(C_1/C_3)^2 - (C_8/3C_3C_5\lambda^2)]^{\frac{1}{2}} \qquad (42)$$

For "a" real, these relations will be satisfied over a finite interval if the quantity in the root is greater than zero. The necessary condition, therefore, that the anti-symmetric component be non zero is that

$$\lambda^2 \geq C_3C_8/3C_1^2C_5 \qquad (43)$$

If condition (43) is not satisfied the load deflection curve is obtained by setting b = 0 in the equilibrium equation (37) thereby obtaining

$$P^* = (C_6/12C_9\lambda)a + (C_3^2\lambda/4C_9)a[a-(C_1/C_3)][a-(2C_1/C_3)] \qquad (44)$$

Such a curve is plotted in Fig. 11. It can be considered to be composed of a straight line due to the bending stress, and to a curve antisymmetrical about $a = C_1/C_3$ due to the axial stress.

This is exactly the same kind of curve as was obtained for the model. The energy load can therefore be obtained from inspection as

$$P^*_e = (1/12\lambda)\ (C_1C_6/C_3C_9) \tag{45}$$

The range of stability can be found from the second variation of the energy. Substituting b = 0 into the total energy (36) and differentiating twice with respect to a yields

$$\frac{\partial^2 H^*}{\partial a^2} = (\lambda/2)[C_1-aC_3)^2 - aC_1C_3 + (a^2C_3^2/2)] + (C_6/12\ ) \tag{46}$$

For stability, this second variation must be greater or equal to zero. Solving for a gives

$$a \leq (C_1/C_3) - [(1/3)(C_1/C_3)^2 - (C_6/9\ C_3{}^2\lambda^2)]^{\frac{1}{2}} \tag{47}$$

or

$$a \geq (C_1/C_3) + [(1/3(C_1/C_3)^2 - (C_6/9\ C_3{}^2\lambda^2)]^{\frac{1}{2}} \tag{48}$$

These portions of the curve are, of course, the portions with a positive slope in Fig. 11. The region of the load deflection curve that is unstable vanishes when the quantity under the root in (47) and (48) becomes zero. An unstable region will therefore exist for

$$\lambda^2 > C_6/3C_1{}^2 \tag{49}$$

and instability will occur after the equality sign in (47) is satisfied. Substituting this value for a into the load deflection relation (44) gives the upper buckling load for the symmetrical

mode.

$$P_U^* = \frac{C_1 C_6}{12 C_3 C_9 \lambda} + \frac{C_3^2 \lambda}{2C_9}\left[\frac{1}{3}\left(\frac{C_1}{C_3}\right)^2 - \frac{C_6}{9C_3^2\lambda^2}\right]^{3/2} \qquad (50)$$

If the inequality (43) is satisfied, b is not identically zero but is given by the expression (40) in the interval given by (41) and (42). Substituting for b from (40) into (37) yields the load deflection relation in this interval.

$$P^* = (C_3 C_8/12\lambda C_5 C_9)[(C_1/C_3) - a] + (1/12\lambda)(C_6 a/C_9) \qquad (51)$$

This is a straight line passing through the energy load $P^* = P_e$ and $a = C_1/C_3$. The total load deflection curve will be then be given by (44) except for the values of a in the interval (41) and (42) where it will be given by (51). This is plotted in Fig.11. The value of a at which the non-symmetrical transition mode comes in, a_T, is obtained from the equal sign in the inequality (41). However, buckling may already have taken place in the symmetrical mode before this value of a is reached. The condition for buckling in the non-symmetrical mode must be

$$a_T \leq a_U$$

where a_U is the deflection at the upper buckling load (Fig. 11). Substituting for a_U and a_T from (47) and (41), upon making both of these inequalities into equalities, gives for $a_T \leq a_U$,

$$\lambda^2 \geq (3C_3 C_8 - C_5 C_6)/6C_1^2 C_5 \qquad (52)$$

The behavior of the arch for different values of λ is

summarized in Fig. 12. The non-symmetrical buckling load P_T^* is obtained by substituting for a in (44) from the equality condition of (41)

$$P_T^* = \frac{C_1 C_6}{12 C_3 C_9 \lambda} + \frac{1}{12\lambda}\left[\frac{C_3 C_8}{C_5 C_9} - \frac{C_6}{C_9}\right]\left[\left(\frac{C_1}{C_3}\right)^2 - \frac{C_8}{3 C_3 C_5 \lambda^2}\right]^{\frac{1}{2}} \qquad (53)$$

The stability of the anti-symmetrical mode can be determined from the slope of the load deflection relation (51). This slope is

$$\frac{dP^*}{da} = (1/12\lambda)[-(C_3 C_8/C_5 C_9) + (C_6/C_9)]$$

which is negative, and hence unstable, for

$$C_3 C_8 > C_5 C_6 \qquad (54)$$

The first term in (53) is the energy load (45), and therefore from (54) and (53) the anti-symmetrical mode will be unstable when

$$P_T^* > P_e^*$$

This result concurs with the general conclusion obtained in the previous section.

(c) Determination of Buckling Loads by Classical Eigenvalue Theory.

The instability of the arch can also be approached by considering small displacements about an equilibrium position as in the classical eigenvalue formulation. The buckling load is determined in this procedure as the load for which geometrically adjacent equilibrium states could exist in addition to the original

state at the same load. Both the upper buckling load P_U and the load for the onset of transitional buckling P_T can be determined by this method.

Denoting the initial state by superscript o and the buckling displacements and strain by superscript ' , the change in strain energy during buckling is

$$U'_m = (1/2) \int_{-\beta}^{\beta} (\varepsilon'^2 + 2\varepsilon'\varepsilon^o) d\alpha$$

$$U'_b = (t^2/24) \int_{-\beta}^{\beta} (\varkappa'^2 + 2\varkappa^o\varkappa') d\alpha \qquad (55)$$

$$U'_p = -(P/EtRf) \left[w'\right]_{\alpha=0}$$

For equilibrium in the buckled state, the variation of the total energy must be zero. The variation with respect to the tangential buckling displacement u' gives simply

$$\varepsilon'_\alpha = 0$$

or by integration

$$\varepsilon' = C' \qquad (56)$$

The buckling strain, which is the difference between the final strain and the strain in the unbuckled state, is therefore a constant. From the definition of the buckling strain, the relation between that strain and the displacements is

$$\varepsilon' = (1/R)(u'_\alpha - w') + (1/2R^2)(w'^2_\alpha + 2w^o_\alpha w'_\alpha) = C' \qquad (57)$$

which, upon solving for u'_α, gives

$$u'_\alpha = w' - (1/2R)(w'^2_\alpha + 2w^o w'_\alpha) + C'R \tag{58}$$

Integrating between $\alpha = \beta$ and $\alpha = -\beta$ and utilizing the clamped boundary conditions ($u = 0$) yields

$$C' = -(1/2R\beta)\int_{-\beta}^{\beta}[w' - (1/2R)(w'^2_\alpha + 2w^o_\alpha w'_\alpha)]d\alpha \tag{59}$$

Substituting this value for C' into (56), the change in energy due to buckling can be written as

$$H' = (1/4R^2\beta)\left\{\int_{-\beta}^{\beta}[w' - (1/2R)(w'^2_\alpha + 2w^o_\alpha w'_\alpha)]d\alpha\right\}^2$$

$$+ (t^2/24R^4)\int_{-\beta}^{\beta}(w'_{\alpha\alpha})^2 d\alpha - \int_{-\beta}^{\beta}\left\{(\epsilon^o/2R\beta)\int_{-\beta}^{\beta}[w' - (1/2R)(w'^2_\alpha + 2w^o_\alpha w')]d\alpha\right\}d\alpha$$

$$+ (t^2/12R^2)\int_{-\beta}^{\beta} x^o w'_{\alpha\alpha}\, d\alpha - (P/EtRf)(w')_{\alpha=0} \tag{60}$$

Because the initial state is an equilibrium state all the linear terms in w must cancel out either algebraically or due to boundary conditions. If it is assumed in addition that w is sufficiently small so that terms of higher order than second can be neglected (in accordance with the basic assumption of classical buckling theory), then the energy change is reduced to

$$H' = (1/4R^2\beta)\left\{\int_{-\beta}^{\beta}[w' - (1/R)w^o_\alpha w'_\alpha)]d\alpha\right\}^2 + (t^2/24R^4)\int_{-\beta}^{\beta} w'^2_{\alpha\alpha}\, d\alpha$$
$$+ (1/2R^2)\varepsilon^o \int_{-\beta}^{\beta} w'^2_\alpha d\alpha \qquad (61)$$

The pre-buckling strain ε^o can be taken outside the integral since it is a constant. Assume that

$$w' = A'w_1 + B'w_2$$

where w_1 is a symmetric function in α and w_2 is anti-symmetric. The functions w_1 and w_2 are therefore orthogonal in the interval $-\beta \leq \alpha \leq \beta$. Substituting into the energy expression (61) gives

$$H' = (1/4R^2\beta)\left\{\int_{-\beta}^{\beta}[A'w_1 + B'w_2 - (1/R)w^o(A'w_{1\alpha} + B'w_{2\alpha})]d\alpha\right\}^2$$
$$+ (t^2/24R^4)\int_{-\beta}^{\beta}[A'w_{1\alpha\alpha} + B'w_{2\alpha\alpha}]^2 d\alpha + (1/2R^2)\varepsilon^o\int_{-\beta}^{\beta}(A'w_{1\alpha} + B'w_{2\alpha})^2 d\alpha \qquad (62)$$

Because of the orthogonality properties, this reduces to

$$H' = A'^2\left\{(1/4R^2\beta)\left[\int_{-\beta}^{\beta}(w_1 - (1/R)w^o_\alpha w_{1\alpha})d\alpha\right]^2 + (t^2/24R^4)\int_{-\beta}^{\beta} w^2_{1\alpha\alpha}d\alpha + (\varepsilon^o/2R^2)\int_{-\beta}^{\beta} w^2_{1\alpha}d\alpha\right\}$$
$$+ B'^2\left\{(t^2/24R^4)\int_{-\beta}^{\beta} w^2_{2\alpha\alpha}d\alpha + (\varepsilon^o/2R^2)\int_{-\beta}^{\beta} w^2_{2\alpha}\, d\alpha\right\} \qquad (63)$$

For equilibrium in the buckled state

$$\frac{\partial H'}{\partial A'} = 0 \qquad \frac{\partial H'}{\partial B'} = 0$$

Each of the two expressions in parentheses in (63) must therefore be zero.

From the second,

$$\varepsilon^o = - (t^2/12R^2) \int_{-\beta}^{\beta} w_{2\alpha\alpha}^2 d\alpha \Big/ \int_{-\beta}^{\beta} w_{2\alpha}^2 d\alpha \tag{64}$$

or, if written in terms of $\xi = \alpha/\beta$,

$$\varepsilon^o = - (t^2/12R^2\beta^2) \int_{-1}^{1} w_{2\xi\xi}^2 d\xi \Big/ \int_{-1}^{1} w_{2\xi}^2 d\xi \tag{65}$$

This gives the strain in the arch when the non-symmetric mode buckling load is reached. From the form of the expression (65) it is seen that the stress is equal to the second mode Euler load of a clamped column of the same length as the arch. By substituting from (27) for ε^o the deflection at buckling can be obtained

$$(1/2R\beta) \int_{-\beta}^{\beta} [w^o - (1/2R) w_\alpha^{o2}] d\alpha = (t^2/12R^2\beta^2) \int_{-1}^{1} w_{2\xi\xi}^2 d\xi \Big/ \int_{-1}^{1} w_{2\xi}^2 d\xi \tag{66}$$

Assuming that $w^o = Aw_1(\xi)$ and introducing the non-dimensional amplitude a defined in (32), and the parameter λ defined by (34) the above expression becomes

$$a^2 \int_{-1}^{1} w_{1\xi}^2 d\xi - 2a \int_{-1}^{1} w_1 d\xi + (1/3\lambda^2) \int_{-1}^{1} w_{2\xi\xi}^2 d\xi \Big/ \int_{-1}^{1} w_{2\xi}^2 d\xi = 0$$

Upon substituting for the integrals from (31),

$$a^2 - (2C_1 a/C_3) + (C_8/3\lambda^2 C_3 C_5) = 0$$

This is the same condition as obtained previously, (41), for the amplitude a_T at which the transitional mode appears.

The first equilibrium equation, obtained by setting the variation of H', (63), with respect to A' equal to zero, can be written, using (27) for ε_o,

$$(1/2\beta)\left\{\int_{-\beta}^{\beta}[w_1 - (1/R)w_\alpha^o w_{1\alpha}]d\alpha\right\}^2 + (t^2/12R^2)\int_{-\beta}^{\beta} w_{1\alpha\alpha}^2 d\alpha$$

$$- (1/2\beta R)\left\{\int_{-\beta}^{\beta}[w^o - (1/2R)w_\alpha^{o2}]d\alpha\right\}\left\{\int_{-\beta}^{\beta} w_{1\alpha}^2 \, d\alpha\right\} = 0 \qquad (67)$$

Again assuming that $w^o = Aw_1$ the equation becomes

$$(1/2\beta)\left\{\int_{-\beta}^{\beta}[w_1 - (A/R)w_{1\alpha}^2]d\alpha\right\}^2 + (t^2/12R^2)\int_{-\beta}^{\beta} w_{1\alpha\alpha}^2 d\alpha$$

$$- (1/2R\beta)\left\{\int_{-\beta}^{\beta}[Aw_1 - (A^2/2R)w_{1\alpha}^2]d\alpha\right\}\left\{\int_{-\beta}^{\beta} w_{1\alpha}^2 d\alpha\right\} = 0 \qquad (68)$$

Using the previous notation, this equation reduces to

$$a^2 - (2C_1 a/C_3) + (2/3)(C_1/C_3)^2 + (C_6/9\lambda^2 C_3^2) = 0$$

which is the same condition as obtained previously for the deflection a_U at the upper buckling load (47). The strain at which this occurs can then be determined from (27). The corresponding load P_U can be obtained by setting $a = a_U$ in the load deflection relation which would be identical to (44).

This analysis shows that although the problem is basically a nonlinear one, both the upper buckling load for symmetrical buckling and the non-symmetrical transitional buckling load can be determined by the classical eigenvalue procedure. The essential difference between this problem and the standard ones is that nonlinear strain displacement relations must be used in describing the pre-buckling states.

(d) Analysis of a Geometrically Imperfect Clamped Arch.

It is of interest to compare the behavior of the clamped arch with initial imperfections with the observations in the preceding general discussion. It will be assumed that the deviations from the perfect circular shape are given by the functions w^e and u^e. The elastic membrane strain can then be written as

$$\varepsilon = (1/R)(u_\alpha - w) + (1/2R^2)(w_\alpha^2 + 2w_\alpha w_\alpha^e) \tag{69}$$

and the change in curvature, as before, is given by (20). The energy expressions (21) (22) and (23) still hold. By varying the total energy with respect to the displacement u, as previously, the axial strain is found to have a constant value given by

$$\varepsilon = -(1/2R\beta)\int_{-\beta}^{\beta}[w - (1/2R)(w_\alpha^2 + 2w_\alpha w_\alpha^e)]\,d\alpha \tag{70}$$

and therefore the total energy can be expressed as

$$H = (1/4R^2\beta)\left\{\int_{-\beta}^{\beta}[w-(1/2R)(w_\alpha^2 + 2w_\alpha w_\alpha^\bullet)]d\alpha\right\}^2 + (t^2/24R^2)\int_{-\beta}^{\beta} w_{\alpha\alpha}^2 d\alpha$$

$$- (P/EtRf)\ (w)_{\alpha=0} \qquad (71)$$

It is assumed that w is given by (29) and the initial imperfections by $w^\bullet = Dw_1(\xi) + Ew_2(\xi)$ where w_1 and w_2 are the same functions as in (29). The total energy can then be written as

$$H^* = (\lambda/4)\left\{aC_1 + bC_2 - (1/2)(a^2C_3 + 2abC_4 + b^2C_5) - [adC_3 + (bd + ae)C_4 + beC_5]\right\}^2$$

$$+ (1/24\lambda)(a^2C_6 + 2abC_7 + b^2C_8) - P^*(aC_9 + bC_{10}) \qquad (72)$$

where the quantities a,b,d,e are non-dimensional amplitudes obtained by dividing the corresponding capitalized quantities by the factor $R\beta^2$, e.g. (32).

Because of the orthogonality of the functions w_1 and w_2,

$$C_2 = C_4 = C_7 = C_{10} = 0$$

H^* therefore can be reduced to

$$H^* = (\lambda/4)[aC_1-(1/2)(a^2C_3 + b^2C_5) - (adC_3 + beC_5)]^2$$

$$+ (1/24\lambda)(a^2C_6 + b^2C_8) - P^*aC_9 \qquad (73)$$

For equilibrium, $\frac{\partial H^*}{\partial a} = 0$, $\frac{\partial H^*}{\partial b} = 0$,

which results in the following two equations:

$$P^{*}C_9 = (\lambda/2)[aC_1-(1/2)(a^2C_3 + b^2C_5)-(adC_3 + beC_5)](C_1-aC_3-dC_3) + (1/12\lambda)(aC_6) \tag{74}$$

$$(\lambda/2)[aC_1-(1/2)a^2C_3 + b^2C_5)-(adC_3 + beC_5)][bC_5 + eC_5] - (1/12\lambda)bC_8 = 0 \tag{75}$$

Unlike the corresponding equation for the geometrically perfect system, (38), b = 0 is no longer a solution. The deformations in the anti-symmetrical mode therefore commences immediately at the onset of loading.

Upon changing the origin in the load deflection plane by the transformation

$$a' = a - [(C_1/C_3) - d] \tag{76}$$

the two equilibrium equations (74) and (75) can be rewritten

$$P^{*}C_9 = - (\lambda/2)\left[(C_3/2)\left\{[(C_1/C_3)-d]^2-a'^2\right\}- [(b^2C_5/2) + beC_5]\right] a'C_3 + (C_6/12\lambda)[a' + (C_1/C_3)-d] \tag{77}$$

$$(\lambda/2)\left[(C_3/2)\left\{[(C_1/C_3)-d]^2-a'^2\right\}-[(b^2C_5/2) + beC_5]\right] (b+e)C_5 - (bC_8/12\lambda) = 0 \tag{78}$$

From (78) it is seen that the amplitude of the anti-symmetric mode b is independent of the sign of a', i.e. b is symmetric about a' = 0. The load deflection relation (77) consists of a membrane contribution (the quantity containing λ) and a bending part (containing $1/\lambda$). The bending term is linear in a' whereas the membrane term is/a cubic in a'/which is anti-symmetrical about and passes through a' = 0. The load deflection curve is therefore composed of a straight line, and a curve anti-symmetrical about $a = [(C_1/C_3)-d]$. The energy load is therefore given by

$$P_e^* = (C_6/12\lambda C_9)[(C_1/C_3)-d] \qquad (79)$$

If the initial imperfections are anti-symmetrical, d = 0, and the energy load is the same as for the geometrically perfect arch (45).

The behavior of the clamped arch is therefore similar to that of the model in that the behavior in the presence of anti-symmetrical imperfections is identical to the type A imperfection of the model. Symmetrical imperfections of the arch would be of type B and correspond to a change in the overall geometry and would result in a change (lowering) of the energy load as noted in (79).

(e) <u>More Exact Solution of the Nonlinear Deformations of the Clamped Arch</u>.

A better approximation to the load deflection relations and to the buckling loads of the arch can be obtained by including more terms in the expression for the deflected shape. Symmetrical deformations will first be considered. The deflected shape is assumed to be given by

$$w = \sum_{n=1}^{r} A_n w_n(\xi) \tag{80}$$

A_n is then the amplitude of the deflection function w_n and $\xi = \alpha/\beta$ as before. Substituting the deflected shape (80) into the expression (28) for the total energy yields

$$H^* = (\lambda/4)\left\{\int_{-1}^{1}\left[\sum_{1}^{r} a_n w_n\right]d\xi - \tfrac{1}{2}\int_{-1}^{1}\left[\sum_{1}^{r} a_n w_{n\xi}\right]^2 d\xi\right\}^2$$

$$+ (1/24\lambda)\int_{-1}^{1}\left[\sum_{1}^{r} a_n w_{n\xi\xi}\right]^2 d\xi - P^*\left[\sum_{1}^{r} a_n w_n\right]_{\xi=0} \tag{81}$$

where

$$a_n = A_n/R\beta^2 \tag{82}$$

If $w_{n\xi}$ and $w_{n\xi\xi}$ form orthogonal sets such that

$$\int_{-1}^{1} w_{n\xi} w_{m\xi} d\xi = 0 \qquad n \neq m$$

and (83)

$$\int_{-1}^{1} w_{n\xi\xi} w_{m\xi\xi} d\xi = 0 \qquad n \neq m$$

The total energy is reduced to

$$H^* = (\lambda/4)\left\{\sum_1^r \left[a_n \int_{-1}^{1} w_n d\xi\right] - \tfrac{1}{2}\sum_1^r \left[a_n^2 \int_{-1}^{1} w_{n\xi}^2 d\xi\right]\right\}^2$$

$$+ (1/24\lambda)\sum_1^r \left[a_n^2 \int_{-1}^{1} w_{n\xi\xi}^2 d\xi\right] - P^* \sum_1^r \left[a_n^2 (w_n)_{\xi=0}\right] \qquad (84)$$

The equilibrium condition is

$$\frac{\partial H^*}{\partial a_n} = 0$$

which leads to r equations of the form

$$(\lambda/2)\left\{\sum_1^r \left[a_n \int_{-1}^{1} w_n d\xi\right] - \tfrac{1}{2}\sum_1^r \left[a_n^2 \int_{-1}^{1} w_{n\xi}^2 d\xi\right]\right\}$$

$$\cdot\left\{\int_{-1}^{1} w_n d\xi - a_n \int_{-1}^{1} w_{n\xi}^2 d\xi\right\} + (1/12\lambda)a_n \int_{-1}^{1} w_{n\xi\xi}^2 d\xi - P^*[w_n]_{\xi=0} = 0 \qquad (85)$$

The following notation is introduced:

$$C_{1n} = \int_{-1}^{1} w_n d\xi \qquad C_{2n} = \int_{-1}^{1} w_{n\xi}^2 d\xi$$

$$C_{3n} = \int_{-1}^{1} w_{n\xi\xi}^2 d\xi \qquad C_{4n} = [w_n]_{\xi=0} \qquad (86)$$

The equilibrium equations for symmetrical deformation of the arch can then be written as

$$(\lambda/2)\left\{\sum_{1}^{r} a_n C_{1n} - \tfrac{1}{2}\sum_{1}^{r} a_n^2 C_{2n}\right\}\left\{C_{1n} - a_n C_{2n}\right\} + (1/12\lambda)a_n C_{3n} - P^* C_{4n} = 0 \quad (87)$$

The criterion obtained previously for the occurrence of anti-symmetrical buckling (66) remains essentially unchanged. The only modification would be that the more general expression (80) would be used to represent the pre-buckled state. This generalization of (66) leads to

$$\sum_{1}^{r} [a_n \int_{-1}^{1} w_n d\xi] - (1/2) \sum_{1}^{r} [a_n^2 \int_{-1}^{1} w_{n\xi}^2] = K/6\lambda^2 \quad (88)$$

where

$$K = \int_{-1}^{1} w_{a\xi\xi}^2 d\xi \Big/ \int_{-1}^{1} w_{a\xi}^2 d\xi \quad (89)$$

and w_a is the anti-symmetrical buckled shape. Upon using the expressions (86) for the constants, the criterion for anti-symmetrical buckling becomes

$$\sum_{1}^{r} a_n C_{1n} - (1/2)\sum_{1}^{r} a_n^2 C_{2n} = K/6\lambda^2 \quad (90)$$

To obtain the anti-symmetrical mode buckling load the set of equations (87) has to be solved simultaneously with (90). Substituting (90) into (87) yields

$$(K/12\lambda)[C_{1n} - a_n C_{2n}] + (1/12\lambda)a_n C_{3n} - P_T^* C_{4n} = 0 \quad (91)$$

which can be solved for a_n

$$a_n = (12\lambda P^* C_{4n} - KC_{1n})/(C_{3n} - KC_{2n}) \qquad (92)$$

This value for a_n can now be substituted back into the buckling criterion (90),

$$(12\lambda P_T^*)^2 \sum_1^r [C_{2n}C_{4n}^2/(C_{3n} - KC_{2n})^2] - (24\lambda P_T^*) \sum_1^r [C_{1n}C_{3n}C_{4n}/(C_{3n}-KC_{2n})^2]$$

$$+ (K/3\lambda^2) + K \sum_1^r [C_{1n}^2(2C_{3n} - KC_{2n})/(C_{3n} - KC_{2n})^2] = 0 \qquad (93)$$

This can be written as

$$(12\lambda P_T^*)^2 D_1 - 24\lambda P_T^* D_2 + (K/3\lambda^2) + KD_3 = 0$$

and therefore the asymmetrical mode buckling load is given by

$$P_T^* = (1/12\lambda)\left\{(D_2/D_1) \pm [(D_2/D_1)^2 - (KD_3/D_1) - (K/3\lambda^2 D_1)]^{\frac{1}{2}}\right\} \qquad (94)$$

where

$$D_1 = \sum_1^r [C_{2n}C_{4n}^2/(C_{3n} - KC_{2n})^2]$$

$$D_2 = \sum_1^r [C_{1n}C_{3n}C_{4n}/(C_{3n} - KC_{2n})^2] \qquad (95)$$

$$D_3 = \sum_1^r [C_{1n}^2(2C_{3n} - KC_{2n})/(C_{3n} - KC_{2n})^2]$$

The second buckling mode can therefore be determined fairly easily by evaluating the C's and D's and solving a quadratic for $12\lambda P^*$.

For a clamped arch a general displacement function that satisfies the boundary conditions is

$$w_n = \tfrac{1}{2}[1 + \cos n\pi\xi], \quad n \text{ odd}$$
$$w_n = \tfrac{1}{2}[1 - \cos n\pi\xi], \quad n \text{ even} \tag{96}$$

This will also satisfy the orthogonality relations (83). The constants (86) can then be readily evaluated.

$$\left.\begin{aligned} C_{1n} &= 1 \\ C_{2n} &= n^2\pi^2/4 \\ C_{3n} &= n^4\pi^4/4 \end{aligned}\right\} \text{ all } n$$
$$C_{4n} = \begin{cases} 1, & n \text{ odd} \\ 0, & n \text{ even} \end{cases} \tag{97}$$

The quantity K is the coefficient in the equation for the second mode buckling load for a clamped column, namely,

$$K = 20.16 \text{ or } 2.0426\pi^2$$

The constants (95) then become

$$D_1 = \sum_1^r [4/n^2\pi^6(n^2-2.0426)^2], \quad n \text{ odd}$$
$$= 0, \quad n \text{ even}$$
$$D_2 = \sum_1^r [4/\pi^4(n^2-2.0426)^2], \quad n \text{ odd} \tag{98}$$
$$= 0, \quad n \text{ even}$$
$$D_3 = \sum_1^r [4(2n^2-2.0426)/n^2\pi^4(n^2-2.0426)^2], \quad \text{all } n$$

The values of these constants are for

$r = 1$:

$D_1 = 4 \times 0.9210/\pi^6$, $D_2 = 4 \times 0.9210/\pi^4$, $D_3 = -4 \times 0.00387/\pi^4$

$r = 2$:

D_1 and D_2 unchanged and $D_3 = 4 \times 0.3498/\pi^4$

For $r = 6$, which is sufficient to determine the constants to 3 figures after the decimal point, the results are

$$D_1 = 4 \times 0.9233/\pi^6, \quad D_2 = 4 \times 0.9436/\pi^4, \quad D_3 = 4 \times 0.3960/\pi^4$$

The anti-symmetrical transitional buckling load can then be readily obtained from (94) for these three cases

$$r = 1$$
$$P_T^* = (\pi^2/12\lambda)\left\{1 + [1.0858 - (0.1847\pi^4/\lambda^2]^{\frac{1}{2}}\right\}$$

$$r = 1$$
$$P_T^* = (\pi^2/12\lambda)\left\{1 + [0.2245 - (0.1847\pi^4/\lambda^2)]^{\frac{1}{2}}\right\}$$

$$r = 6$$
$$P_T^* = (\pi^2/12\lambda)\left\{1.0219 + [0.1685 - 0.1843\pi^4/\lambda^2]^{\frac{1}{2}}\right\}$$

These three functions are plotted in Figure 13. There is an appreciable difference between the curves for 1 and 2 terms, but not much between the curves for 2 and 6 terms.

Determining the upper buckling load for the symmetrical mode, P_U, is somewhat more involved. It is therefore only attempted for $r = 1$ and $r = 2$. For $r = 1$ the upper buckling load is obtained immediately by substituting the constants (97) into the expression for one term obtained previously (50) observing that

$$C_{1n} = C_1,\ C_{2n} = C_3,\ C_{3n} = C_6,\ C_{4n} = C_9 \quad \text{when } n = 1$$

This gives

$$P_U^* = (\pi^2/12\lambda) + (\lambda\pi^4/4)\left[(4/3\pi^4) - (1/9\lambda^2)\right]^{3/2} \tag{99}$$

The energy load for a single term is obtained by substituting the values of the constants into (45) thereby obtaining

$$P_e^* = \pi^2/12\lambda \tag{100}$$

The next approximation, r = 2 will be considered. From the equilibrium equations (87) it is seen that

$$\frac{P^*C_{4n} - (a_nC_{3n}/12\lambda)}{C_{1n} - a_nC_{2n}} = \frac{P^*C_{4m} - (a_mC_{3m}/12\lambda)}{C_{1m} - a_mC_{2m}}$$

which can be solved for a_n in terms of a_m and the load P^*

$$a_n = \frac{P^*(C_{4n}C_{1m} - C_{1n}C_{4m} - a_mC_{4n}C_{2m}) + a_m(C_{1n}C_{3m}/12\lambda)}{-P^*C_{2n}C_{4m} + (a_m/12\lambda)(C_{2n}C_{3m} - C_{3n}C_{2m}) + (C_{1m}C_{3n}/12\lambda)}$$

For r = 2 this reduces to

$$\pi^2 a_2 = -(k_1 - P^*)/(k_2 + P^*) \tag{101}$$

where

$$k_1 = a/48\mu,\ k_2 = 1/\mu[(a/16) - (1/3)],$$
$$a = \pi^2 a_1, \text{ and } \mu = \lambda/\pi^2 \tag{102}$$

The first of the equilibrium equations (87) can then be written as

$$[\pi^2 a_1 + \pi^2 a_2 - (a_1^2\pi^4/8) - a_2^2\pi^4/2)]\ [1 - (a_1\pi^2/4)]$$

$$+ (a_1\pi^6/24\lambda^2) - (2\pi^2 P^*/\lambda) = 0 \qquad (103)$$

Upon substitution for $\pi^2 a_2$ from (101) and the use of the notation (102), a relation between a and P^* can be obtained. This is

$$\left\{[a-(a^2/8)](k_2 + P^*)^2 - (k_1 - P^*)(k_2 + P^*) - (1/2)(k_1 - P^*)^2\right\}[1-(a/4)]$$

$$+ [(a/24\mu^2) - (2P^*/\mu)](k_2 + P^*)^2 = 0 \qquad (104)$$

The load deflection relation for symmetrical deformation is given explicitly by this expression. Because of the complexity of the expression, the load deflection curve can be best determined by first introducing new variables $\bar{a}$ and p defined as follows:

$$\bar{a} = a - 4 \qquad p = 48\mu P - 4 \qquad (105)$$

Equation (104) can then be written as

$$K_o + K_1 p + K_2 p^2 - 4p^3 = 0 \qquad (106)$$

where

$$\begin{aligned} K_o &= \bar{a}^3[36 + 3\mu^2(9\bar{a}^2 - 116)] \\ K_1 &= \bar{a}^2[-12 + 3\mu^2(6\bar{a}^2 - 120)] \\ K_2 &= \bar{a}[-20 + 3\mu^2(\bar{a}^2 - 20)] \end{aligned} \qquad (107)$$

The solution to (106) is antisymmetrical in p about the origin $\bar{a} = p = 0$. The energy load is therefore immediately

obtained as

$$p_e = 0$$

or from (105) and (102)

$$P_e^* = \pi^2/12$$

The energy load is therefore unchanged by going from 1 to 2 terms in the expansion for the deflected shape. The addition of the second term is found not to alter the relation between the load and the bending deformation and the symmetry of the membrane stresses. The influence of the second term is therefore similar to that of a type A imperfection. This result would probably not be true by the inclusion of more terms in the deflected shape function, but it is believed that the consideration of additional terms will not have any significant effect on the energy load.

The upper buckling load for the symmetrical mode is most easily obtained by plotting p against $\bar{a}$, and determining the value of p at the limit point from the resulting plot. This value can be transformed back to the original coordinates using (105) and (102). Performing this procedure for a range of the geometric parameter λ, a plot of P_U^* against λ is obtained. This is shown in Figure 13 along with the energy load, the one term approximation for P_U^*, and the transitional buckling load P_T^*.

(f) Experiments on Elastic Snap Buckling of Clamped Arches.

The experimental part of the study was concerned with obtaining complete load deflection curves for a wide range of geometries of clamped arches. It was of special interest to obtain the unstable regions of these curves and to investigate the mode shapes at various stages of loading. The experimental setup was constructed so that creep snap buckling tests as well as elastic tests were possible. In this section only the elastic tests conducted at room temperature are considered. Figure 14 shows a schematic drawing of the apparatus and Fig. 15 and 16 are photographs of the actual apparatus.

The arch was clamped between two fixing blocks at each end. It was necessary to make a series of these blocks of different angles to cover the range of geometry. The fixing blocks were bolted to a very stiff auxiliary frame which rested freely upon the main support frame. This was necessary to allow the auxiliary frame to expand freely for the high temperature tests. To ensure complete rigidity of the clamping, the fixing blocks were backed up against two other blocks which were bolted and doweled to the auxiliary frame.

The deformations of the arch were measured at several points with dial gauges. These were arranged outside the furnace with extension rods resting on the arch. The extension rods were counterweighted with springs to minimize the effect of their weight on the behavior of the arch. Experiments with only the center gauge and all the gauges confirmed that this was achieved.

The load was applied at the center through a knife edge fixture and a loading rod extending out of the furnace. To obtain the complete load deflection curve, a system of a jack and a strain gauge instrumented load cell in series with the applied load was utilized. The load, which was greater than P_U, rested upon the jack and the entire load deflection relation was obtained by lowering the jack in small increments - in effect a deflection controlled procedure - and noting the load supported by the arch from the load cell and the corresponding deflections from the dial gauges.

The specimens were made from 2024T4 aluminum alloy and were one inch wide, three sixteenths inches thick, and nominally 34 inches between supports. They were rolled into a circular arc using a three roller sheet metal roll. The geometry was determined by measuring the central height after the specimens were bolted into the auxiliary frame. The clamping resulted in a slight pre-stressing for some of the specimens, particularly at the lower values of λ, as it was very difficult to get the angle of the fixing blocks to coincide exactly with the base angle of the specimens.

In all, 14 specimens were tested for λ ranging from 3.69 to 16.25. Table I gives the geometries and the buckling loads obtained. All the experiments were completely elastic as the specimens were found to return to their original shape to within a few thousandths of an inch upon unloading. The lower buckling load of the clamped arch is greater than zero and therefore the arch cannot remain in the buckled state when the load is removed.

The experimental buckling loads (the maximum points in the load deflection curves) are compared with the theoretical results

in Fig. 13. Except for the two points with the lowest values of λ, the agreement with the two term solution is very good. It is probable that the disagreement in those two cases was due to the clamping stresses.

Fig. 17 shows complete load - central deflection curves for three values of λ along with corresponding theoretical predictions. The complete theoretical load deflection curves (for 1 and 2 terms) are shown for the $\lambda = 11.62$ case. Although the general trends and especially the buckling load values are in close agreement, the curves by themselves are not conclusive as to the buckling mode in the unstable region. It is noted, however, that for large λ, P_U is appreciably greater than P_T and the experiments agree, as expected, with P_T.

Although the anti-symmetrical mode governs the buckling process for $\lambda > 10.6$, the actual amplitude of the anti-symmetrical mode is relatively small and could be readily overlooked in a superficial test. The shapes at buckling for various arches are shown in Fig. 18. The increased waviness in the shapes for the larger λ values and the corresponding need for more than one term in the theoretical solution can be readily noted. The asymmetry of the shapes can be noticed for the large λ values but is very small compared to the overall symmetrical deformation. Fig. 19 shows the deflected shapes for two values of λ at the upper, lower, and middle buckling points. Even at the middle buckling position, when the anti-symmetrical amplitude is largest, the asymmetry is small for the $\lambda = 16.25$ case and almost non-existent, as expected, for $\lambda = 5.35$. These results show that although the buckling of a

system may be governed by anti-symmetrical modes, these modes may not be readily detectable except by very careful experimentation. These observations are believed to be pertinent to the related problem of the buckling of spherical caps.

(g) General Discussion of Results for the Clamped Arch.

1. The experimental results were in good agreement with the general theoretical predictions and showed that for large λ buckling is governed by anti-symmetrical modes - the buckling load corresponded to the transitional buckling values P_T. The amplitudes of the anti-symmetrical modes were, however, relatively small. As expected, the energy load was a lower bound on the experimental buckling loads, and could have served to give reasonable predictions.

2. Although a change in buckling mode occurs (theoretically) at $\lambda = 10.6$, the transition is a smooth one and the buckling load-geometry (λ), curve is also smooth. The behavior is therefore unlike the sharp divisions obtained for plate buckling, and is a further reason for the difficulty in detecting buckling mode changes.

3. The general features of the nonlinear behavior of the clamped arch were found to be similar to those of the simple mechanical model and to conform with the general results obtained for such nonlinear systems.

4. The one term solution gave the proper overall behavior but was appreciably in error on the actual magnitudes especially for the higher values of λ. The two term solution gave fairly good results - the additional corrections to the six term solution for the anti-symmetrical buckling load are relatively small.

5. The energy load was the same for both the one and two term solutions. Although the energy load would not be unchanged in the complete solution, there are strong indications that the energy load is a relatively insensitive function of the buckled shape.

Creep Buckling of Arches.

The creep buckling problem was studied as an important problem in its own right and as an example in a difficult field where the energy load concepts may have application. The possibility that the energy load, as defined for the initial geometry, may be a lower bound on the load required for snap buckling in the presence of creep was the point of particular interest. However, it became evident early in the work that the energy load based on the initial geometry was not a lower bound in the above sense. The only significance of the energy criterion in creep problems, at least for the model and the arch, is that the "membrane" forces corresponding to the original energy load must be exceeded before buckling can occur.

Considerable insight into the snap creep buckling problem can be obtained from the analysis of the simple model of Fig. 2. A related study was performed by Hult [18], but his model did not contain the central spring which would correspond to the bending rigidity in the case of the arch. The energy load for Hult's model is therefore identically zero for all geometries and cannot be used to investigate the significance of the energy load in creep snap buckling problems. In addition Hult's model is statically determinate whereas the force distribution in the more general model depends upon the relative stiffnesses and the creep law as well as upon the geometry.

The problem of creep snap buckling can be formulated as the determination of the load deflection curve for superimposed loading at successive stages of creep of the system. When the geometry and force distribution is such that the load increment required to reach

either P_U or P_T (whichever is lower) becomes zero, then snap buckling will occur. The analysis is based upon assuming that the superimposed load deflection curve can be calculated from elastic theory. The incremental stresses and strains due to buckling are taken to be elastic. This assumption agrees with the commonly used creep laws since the snap buckling process is relatively rapid.

The equilibrium equation for the model of Fig. 2, as given by (2), can be written with slightly greater generality as

$$P = F + 2T(a-\delta)/L \tag{108}$$

where F is the force in the compressed spring, and the other symbols are as defined previously. The strain in the arms is given by (3). In the following analysis it is convenient to consider compressive strains as positive. Both the arms and the spring are considered to creep under the applied forces.

The model is subjected to a constant applied load P_c. The forces in the arms and in the spring, and the apex deflection at any later time are designated T_c, F_c and δ_c respectively. These quantities are also related through (108). The load deflection relation for an additional load P can now be obtained.

The total force in the spring due to $P_c + \Delta P$ is

$$F = F_c + k(\delta - \delta_c)$$

where δ is the total displacement from the unloaded position. From the strain expression (3), the total force in the arms is

$$T = T_c + (AE/2L^2)(\delta - \delta_c)(2a - \delta - \delta_c)$$

The total forces must also satisfy the overall equilibrium equation (108). Upon substitution of the above expressions for F and T into (108) and subtracting the equilibrium conditions for the original loading state, the load deflection relation for the additional load ΔP is obtained as

$$\Delta P = [k-(2T_c/L)](\delta-\delta_c) + (AE/L^3)(a-\delta)(\delta-\delta_c)(2a-\delta-\delta_c) \quad (109)$$

ΔP is plotted against δ in Fig. 20. This is the instantaneous load deflection curve for the system at any stage of creep. The curve again consists of a straight line and a curve antisymmetrical about $\delta = a$. The energy load is therefore

$$\Delta P_e = [k-(2T_c/L)](a-\delta_c) \quad (110)$$

For the fully elastic case this result agrees, as expected, with that obtained by subtracting (2) from the elastic energy load, $P_e = ka$, (9). The energy load for additional loading, ΔP_e, is zero when

$$T_c = kL/2 \quad (111)$$

which, from (9) and (2), is also the value for the force in the arms (the "membrane" force) at the elastic energy load P_e. The condition $\delta_c = a$ is a special case for the vanishing of ΔP_e.

The upper buckling load for the additional load ΔP is found by setting $d(\Delta P)/d\delta = 0$. This yields the following quadratic equation for the total deflection δ_U at buckling

$$3\delta_U^2 - 6a\delta_U - \delta_c^2 + 2a\delta_c + 2a^2 + (L^3/AE)[(k-(2T_c/L)] = 0$$

The upper buckling load condition will be reached by the system with no additional load being required ($\Delta P = 0$) when $\delta_U = \delta_c$, or when

$$T_c = (kL/2) + (AE/L^2)(\delta_c - a)^2 \qquad (112)$$

This has an absolute minimum at $T_c = kL/2$. The minimum value that the force in the arms could have at the upper buckling point for any arbitrary loading path is therefore the same as at the energy load for the fully elastic case.

The transitional buckling condition is reached when the force in the arms equals the Euler buckling load, $T = T_E$. For snap buckling to occur for additional loading above P_c, the additional load must be greater than ΔP_e, (110). The total force in the arms must therefore exceed kL/2 if buckling of the arms is to lead to snap buckling and not to only a bifurcation of equilibrium with a continuously increasing deflection. Fig. 21 shows the combinations of the force in the arms and the displacement that will cause instability. The relative values of the different criteria depend upon the original geometry and the elastic constants, but not on the creep properties. The relation between T_c and δ_c for completely elastic deformation is given by (4) and is also plotted in Fig. 21. The system described by Fig. 21 would buckle under elastic loading when the elastic curve crosses the curve for the limit point (the upper buckling load) condition, point Q.

For the creep problem the system is first loaded elastically up to some point A along the elastic response curve OQ. The

system then creeps under the constant load with consequent changes in the force in the arms and in the deflection. The relation between these two quantities during creep (path AB) depends upon the particular creep law and would result in snap buckling when the values agree with one of the buckling criteria determined previously, e.g., point B in Fig. 21. Although the law for metallic creep is nonlinear, the principal features of the problem can be most easily obtained from the study of linear viscoelastic behavior.

The creep laws for the spring and the arms of the model can be taken as

$$\dot{\delta}_c = (\dot{F}_c/k) + \lambda F_c \tag{113}$$

$$\dot{\varepsilon} = (1/A)[(\dot{T}_c/E) + \mu T_c] \tag{114}$$

where λ and μ are material constants.

Upon differentiating (3) (with the sign changed) with respect to the time, the strain rate in the arms can be obtained as a function of the displacement,

$$\dot{\varepsilon} = (1/L^2)\dot{\delta}_c(a-\delta_c)$$

which, upon substitution into (114), gives

$$\dot{\delta}_c(a-\delta_c) = (L^2/A)[(\dot{T}_c/E) + \mu T_c] \tag{115}$$

Differentiation of the equilibrium equation (108) with respect to the displacement δ_c gives

$$\frac{dF_c}{d\delta_c} = (2/L)[T_c - (a-\delta_c)\frac{dT_c}{d\delta_c}] \tag{116}$$

since the applied load P_c is constant during the creep process. Using the relationship

$$\dot{F}_c = \dot{\delta}_c \frac{dF_c}{d\delta_c} \tag{117}$$

in (113), and solving for the displacement rate gives

$$\dot{\delta}_c = \lambda F_c/[1-(1/k)\frac{dF_c}{d\delta_c}] \tag{118}$$

Substituting for F_c and $\frac{dF_c}{d\delta_c}$ from (108) and (116) leads to the following expression for the deflection rate:

$$\dot{\delta}_c = \frac{\lambda P_c - (2\lambda/L)(a-\delta_c)T_c}{1-(2/kL)[T_c-(a-\delta_c)\frac{dT_c}{d\delta_c}]} \tag{119}$$

Using the relation

$$\dot{T}_c = \dot{\delta}_c \frac{dT_c}{d\delta_c}$$

equation (115) can also be solved for the deflection rate to give

$$\dot{\delta}_c = \frac{(L^2\mu/A)T_c}{(a-\delta_c)-(L^2/AE)\frac{dT_c}{d\delta_c}} \tag{120}$$

Buckling will take place when $\dot{\delta}_c$ becomes infinite or when the denominators of (119) or (120) becomes zero. The buckling criterion is therefore

$$1-(2/kL)[T_c-(a-\delta_c)\frac{dT_c}{d\delta_c}] = 0 \tag{121}$$

$$(a-\delta_c) - (L^2/AE)\frac{dT_c}{d\delta_c} = 0 \tag{122}$$

Solving (121) and (122) simultaneously for T_c gives the same instability locus in the T_c, δ_c, plane as was obtained previously (112) by the additional loading approach. The equation for the creep locus in the T_c, δ_c plane (path AB) can be obtained by equating the two creep rates in (119) and (120). This gives

$$\frac{dT_c}{d\delta_c} = \frac{(\lambda/\mu)(a-\delta_c)[P_c-(2T_c/L)(a-\delta_c)]+(2T_cL/Ak)[T_c-(kL/2)]}{(\lambda/\mu)(L^2/AE)[P_c-(2T_c/L)(a-\delta_c)]+(2T_cL/Ak)(a-\delta_c)} \quad (123)$$

The required locus can be obtained by integrating (123). The initial condition is the solution for the initial elastic loading (point A of Fig. 21). When point B is reached the system will snap through to some point C and creep again along CD. The time necessary to reach B, the creep buckling time, can be computed from (123) and (119) or (120).

The slope of the creep locus can be seen to be positive over most of the T_c, δ_c plane. The term

$$P_c-(2T_c/L)(a-\delta_c)$$

in (123) is equal to F_c from the equilibrium equation (108) and is therefore always positive. The quantity $(a-\delta_c)$ is also positive for $\delta_c < a$. The denominator of (123) is therefore always positive in the region $0 \leq \delta_c \leq a$ for all T_c. The first term in the numerator of (123) is also positive in this region. The second term is positive for $T_c \geq kL/2$ for all δ_c, and negative for $T_c < kL/2$. The slope of the creep locus in the T_c, δ_c plane will therefore be zero or negative for $T_c < kL/2$ when

$$(\lambda/\mu)(a-\delta_c)[P_c-(2T_c/L)(a-\delta_c)]+(2T_cL/Ak)[T_c-(kL/2)] \leq 0 \qquad (124)$$

or in the region below EF in Fig. 21. The lowest initial point that will lead to buckling will be some point G for which the creep locus will be GF which passes through F with a horizontal slope. Initial loading to any point above G will lead to buckling. Since T_c for point G would, in general, be less than the force in the arms at the energy load, loads below the energy load could result in snap buckling of the system.

T. H. H. Pian and C. Y. Chow [19] studied the creep buckling of a simply supported low arch. To simplify the analysis they assumed that the stress distribution across the arch is linear, and that the stresses and displacements varied along the arch in the same manner as in the elastic solution. The second of these conditions is equivalent to assuming that the deformed shape is the same in the elastic and creep processes. They solved the problem using one symmetrical and one asymmetrical term in the deflection function. For symmetrical creep deformations they found the arch to behave in exactly the same manner as the model. They used a creep law of the form

$$\dot{\varepsilon} = (\dot{\sigma}/E) + \mu\sigma^n$$

with n = 1 and 3.

As no experimental results were obtainable in the literature, it was felt that some experiments would be very desirable in view of the many simplifying assumptions made in the analyses. A series of tests were therefore performed on clamped arches in the testing setup described previously. The material used was 5052-O

aluminum. This was selected because at a constant elevated temperature its mechanical properties are fairly constant with time. The specimen was mounted in the oven at room temperature. One end was left loose and free to expand so that no thermal stresses would be induced upon heating. After the oven and the specimen had reached the test temperature, 500°F, and held there for 2-3 hours to ensure uniform temperature, the specimen was clamped. This was made possible by putting extensions on the clamping bolts reaching out of the oven. The dial gauges were then lowered and the dead load applied at the arch center. In order to read all the gauges and the time simultaneously, the gauges and a clock were all photographed at regular intervals. This method proved successful and the deflected shape right up to the time of buckling was obtained for all the tests. In Table II the loads and the geometry of the arches are shown with the time required for buckling to occur. The geometries fall in one group around $\lambda = 9$ and one around $\lambda = 16$. All the tests were performed at loads below the energy load based on the original geometry.

It is interesting to note tests number 1 and 4 where the geometry and the load is the same but the buckling times differ by a factor of ten. One of the reasons for this can be seen in Fig. 22, where the deflection just prior to buckling for the two tests are plotted. Specimen number 4, the one with the longest buckling time, is almost symmetrical whereas number 1 has a large unsymmetrical component.

Fig. 23 shows the deflections for specimen number 7 at three different times. In both Figs. 22 and 23 the importance of including a second symmetrical term in the displacement function is brought out. This is the same as was found for the completely elastic case. The inclusion of such terms would,however,make the creep analyses quite complex. A simplification may be obtained by replacing the arch with a structure of the kind shown in Fig. 24 with six elastic-creep hinges. The deflected shape of such a system would closely resemble the real shapes shown in Figs. 22 and 23 for symmetrical deformations. Fig. 25 shows a buckled arch which shows clearly the sharp hinges formed at the center and at the ends. The possibility of an analyses on these lines will be investigated in a later paper.

Acknowledgment

The authors would like to express their appreciation to Mr. Robert R. Stanton for his valuable assistance in the experimental work.

References

1. Karman, T. von and Tsien, H. S., "The Buckling of Spherical Shells by External Pressure," J. Aero. Sci., vol. 7, no. 2, p. 43, 1939.

2. Karman, T. von and Tsien, H. S., "The Buckling of Thin Cylindrical Shells under Axial Compression," J.Aero. Sci., vol. 8, no. 8, p. 302, 1941.

3. Karman, T. von, Dunn, L. G. and Tsien, H. S., "The Influence of Curvature on the Buckling Characteristics of Structures," J.Aero. Sci., vol. 7, no. 7, p. 276, 1940.

4. Friedrichs, K. O. "On the Minimum Buckling Load for Spherical Shells," Theodore von Karman Anniversary Volume, California Institute of Technology, p. 258, 1941.

5. Tsien, H. S. "Buckling of a Column with Nonlinear Lateral Supports," J. Aero. Sci., vol. 9, no. 4, p. 119, 1942.

6. Tsien, H. S., "A Theory for the Buckling of Thin Shells," J.Aero. Sci., vol. 9, no. 10, p. 373, 1942.

7. Lo, H., Crate, H. and Schwarz, E. B., "Buckling of Thin-Walled Cylinder under Axial Compression and Internal Pressure," NACA TN 2021, 1950.

8. Fung, Y. C., and Sechler, E. E., "Instability of Thin Elastic Shells," Structural Mechanics, Proc. of First Symp. on Naval Structural Mechanics, Pergamon Press, New York, p. 115, 1960.

9. Kaplan, A. and Fung, Y. C., "A Nonlinear Theory of Bending and Buckling of Thin Elastic Shallow Shells," NACA TN 3212, 1954.

10. Fung, Y. C. and Kaplan, A., "Buckling of Low Arches and Curved Beams of Small Curvature," NACA TN 2840, 1952.

11. Keller, H. B. and Reiss, E. L., "Spherical Cap Snapping," J. Aero. Space Sci., vol. 26, no. 10, p. 643, 1959.

12. Budiansky, B., "Buckling of Clamped Shallow Spherical Shells," Proc. of the I.U.T.A.M. Symp. on the Theory of Thin Elastic Shells, No. Holland Pub. Co., Amsterdam, p. 64, 1960.

13. Thurston, G. A., "A Numerical Solution of the Nonlinear Equations for Axisymmetric Bending of Shallow Spherical Shells," J. Appl. Mech., vol. 28, no. 4, p. 557, 1961.

14. Marguerre, K., "Die Durchschlagkraft eines schwach gekrummten Balkens," Sitzber, der Berliner Math. Gesellschaft, vol. 37, 1938; see also Margueere, K., Neuere Festigkeitsprobleme des Ingenieurs, Ch. 5; Julius Springer, Berlin, 1950.

15. Donnell, L. H. and Wan, C.C., "Effect of Imperfections on Buckling of Thin Cylinders and Columns under Axial Compression," J. Appl. Mech., vol. 17, no. 1, p. 73, 1950.

16. Donnell, L. H., "Effect of Imperfections on Buckling of Thin Cylinders under External Pressure," J. Appl. Mech., vol. 23, no. 4, p. 569, 1956.

17. Biezeno, C. B. and Grammel, R., "Engineering Dynamics, vol.II," Blackie and Sons Ltd., London, pp. 397-411, 1956.

18. Hult, J., "Oil Canning Problems in Creep (I)," Publ. No. 130, Institutionen för hällfasthetslära, Kungl. Tekniska Högskolan, Stockholm, 1960 (presented at I.U.T.A.M. Colloq. on Creep in Structures, Stanford Univ., July 1960).

19. Pian, T. H. H. and Chow, C. Y., "Further Studies of Creep Buckling of Curved Beam under Lateral Loading," Technical Report 25-28, Aeroelastic and Structures Lab., M.I.T., December 1958. (see also Pian, T.H.H., "Creep Buckling of Curved Beam under Lateral Loading" Proc. U. S. National Congress of Applied Mechanics, 1958).

Table I

Dimensions and Experimental
Buckling Loads of Clamped Arches

Height (inches)	$\lambda = (\beta^2 R/t)$	P (lb.)
0.346	3.69	no buckling
0.346	3.69	9.05
0.502	5.35	12.15
0.552	5.89	13.70
0.705	7.52	18.10
0.751	8.01	20.85
0.885	9.44	21.30
0.890	9.50	23.90
1.080	11.51	28.45
1.090	11.62	29.65
1.236	13.15	36.20
1.288	13.75	33.30
1.430	15.25	42.00
1.522	16.25	39.50

Horizontal distance between ends = 34 inches
Width = 1 inch; Thickness = 3/16 inch
Material: 2024-T4 Aluminum alloy

TABLE II

Dimensions and Creep Buckling Times for Clamped Arches

No.	Height (inches	λ ($\beta^2 R/t$)	Theoretical Buckling Load(lb.) P_U or P_T (2 term sol.)		Energy Load(lb.) (2 term sol.)	Experimental Applied Load(lb.)	Time for Creep Buckling
1	0.874	9.32	19.2	(P_U)	15.7	14.65	2 min, 34 sec.
2	1.020	10.90	24.0	(P_U)	18.4	14.65	9 min, 25 sec.
3	0.795	8.48	17.8	(P_U)	14.3	14.65	5 min, 12 sec.
4	0.872	9.31	19.1	(P_U)	15.6	14.65	21 min, 9 sec.
5	1.538	16.40	38.7	(P_T)	27.4	21.67	0 min, 50 sec.
6	1.562	16.65	39.4	(P_T)	28.0	11.77	did not buckle
7	1.363	14.53	33.7	(P_T)	24.3	14.65	28 min, 12 sec.
8	1.622	17.10	40.3	(P_T)	28.2	16.65	22 min, 33 sec.

Horizontal distance between ends = 34 inches
Width = 1 inch; Thickness = 3/16 inch
Material: 5052-0 Aluminum Alloy
Test Temperature: 500°F; $E = 8.15 \times 10^6$ lb./sq.in.

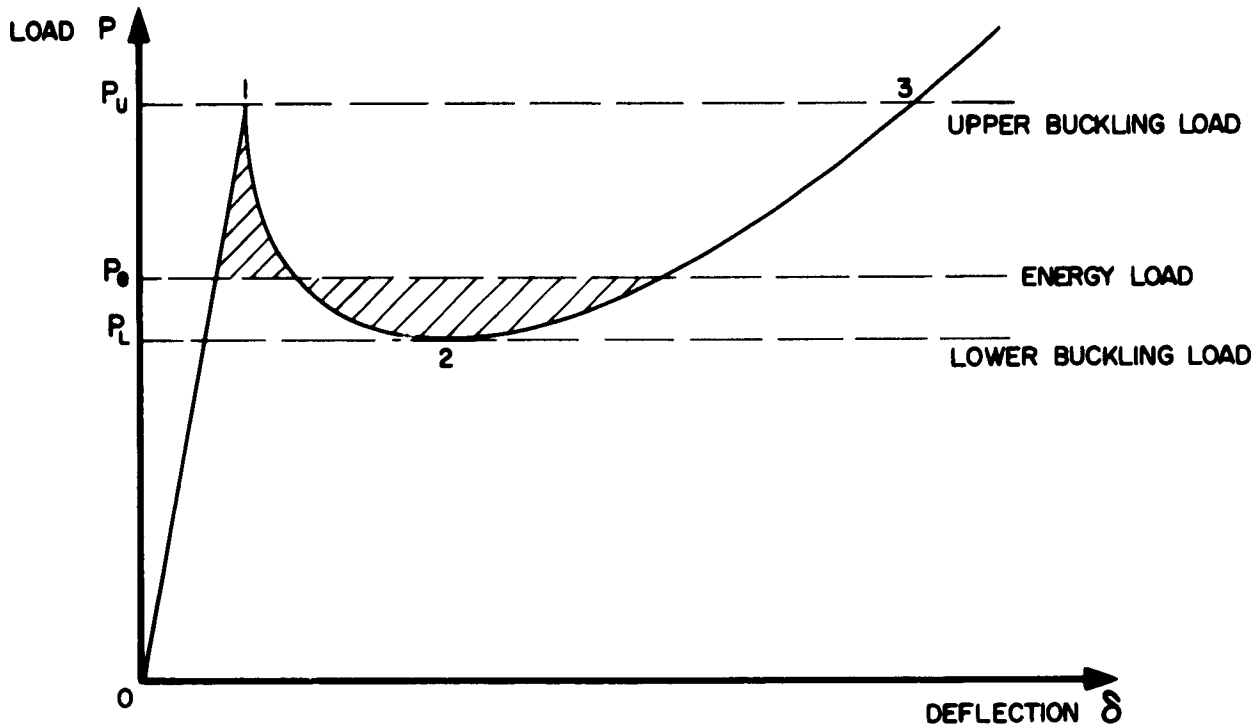

FIG. 1 TYPICAL LOAD DEFLECTION CURVE FOR SYSTEM THAT EXHIBITS SNAP BUCKLING.

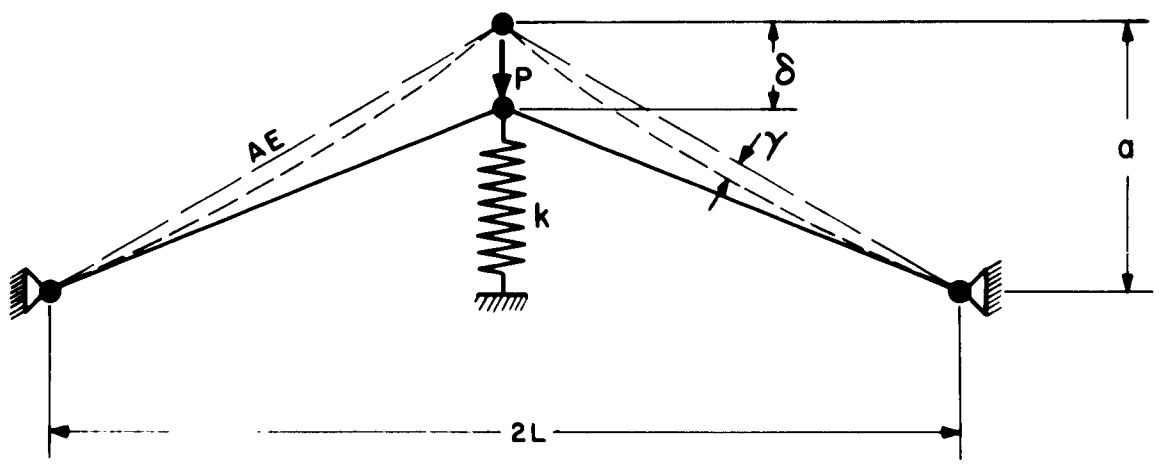

FIG. 2 MODEL TO EXIBIT SNAP BUCKLING.

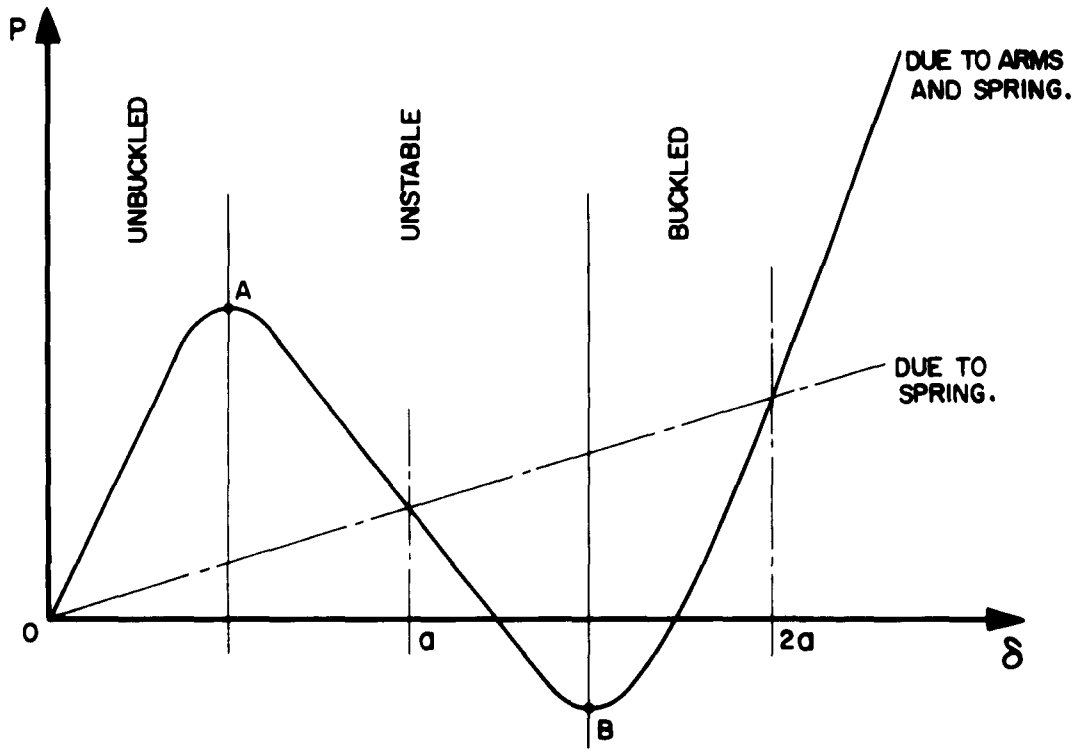

FIG. 3 LOAD DEFLECTION CURVE FOR MODEL.

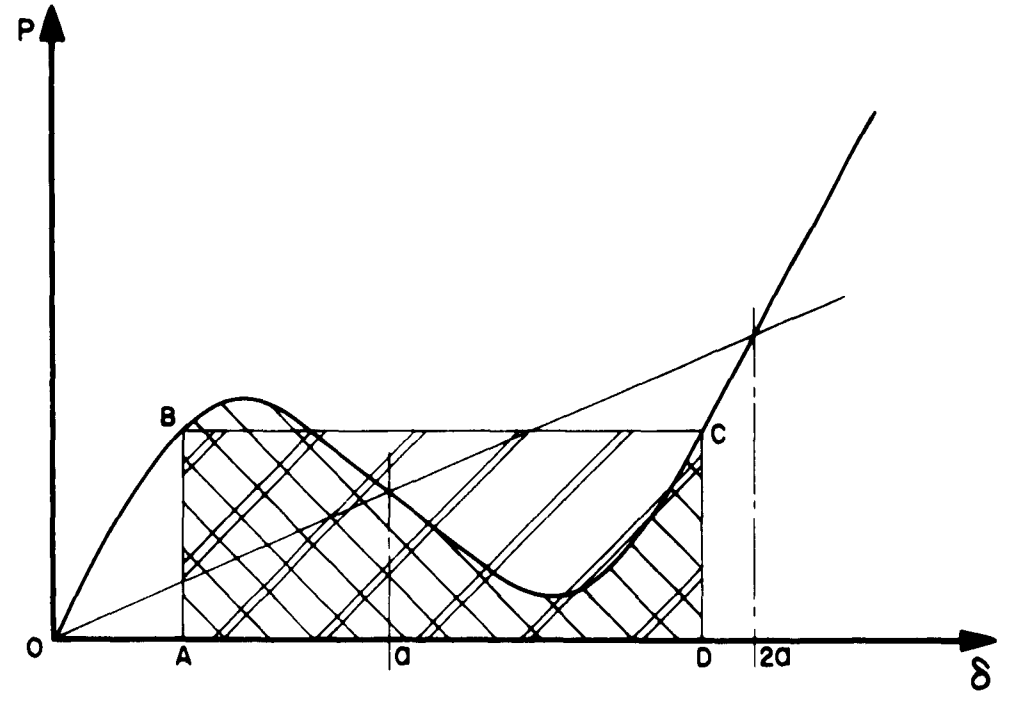

FIG. 4 GRAPHICAL DETERMINATION OF ENERGY LOAD FOR THE MODEL.

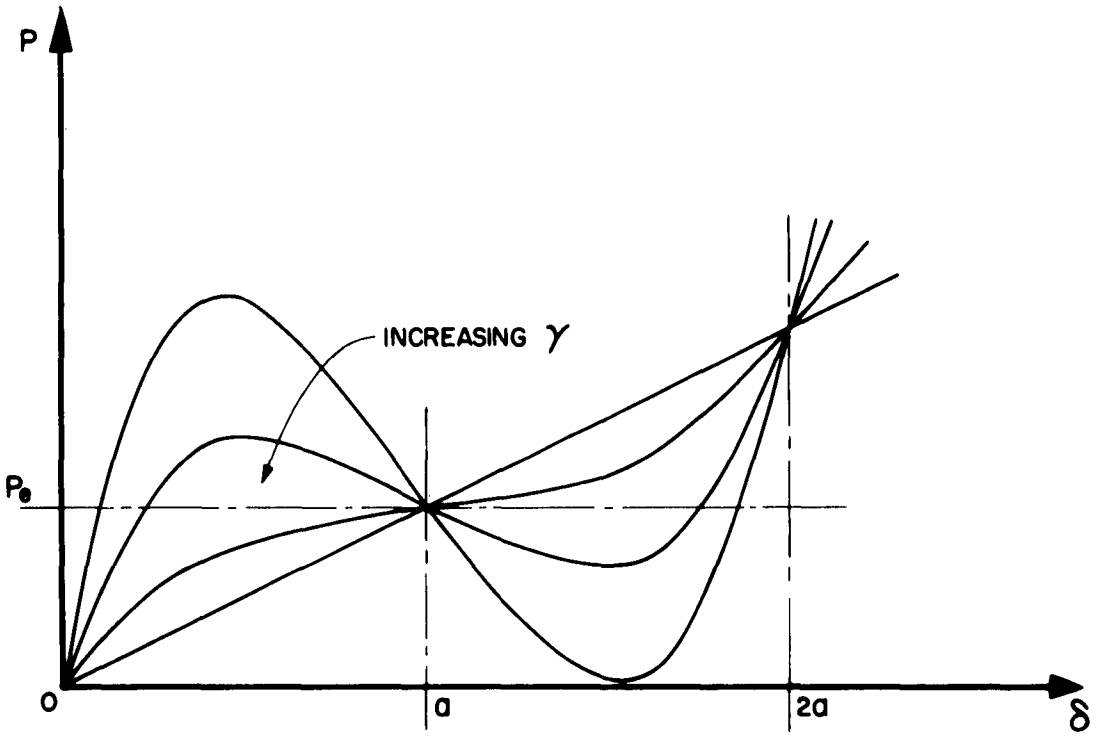

FIG.5 LOAD DEFLECTION CURVES FOR MODEL WITH INITIAL IMPERFECTIONS.

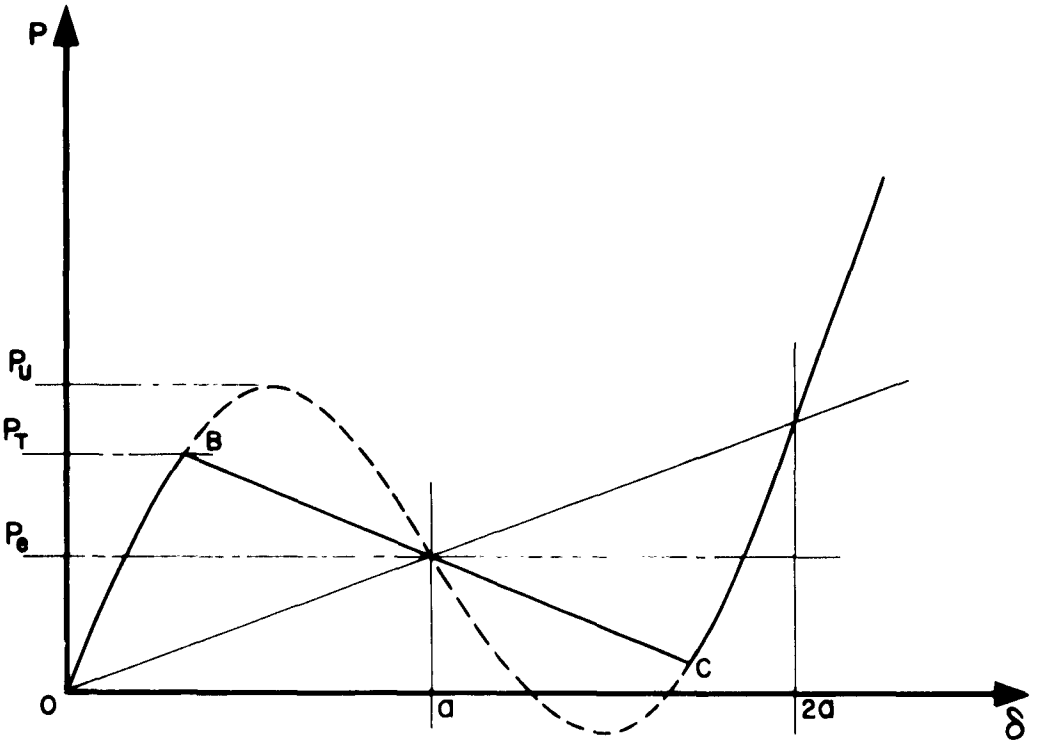

FIG.6 LOAD DEFLECTION CURVE FOR THE MODEL SHOWING NON-SYMMETRICAL BUCKLING PATH.

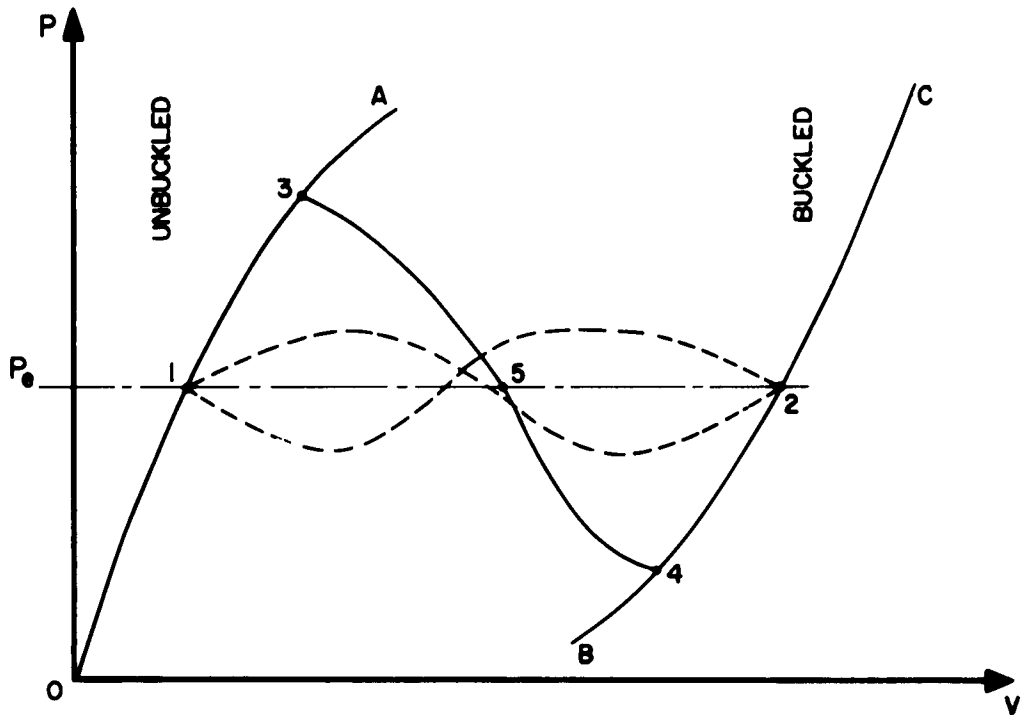

FIG.7 GENERALIZED LOAD DEFLECTION CURVE.

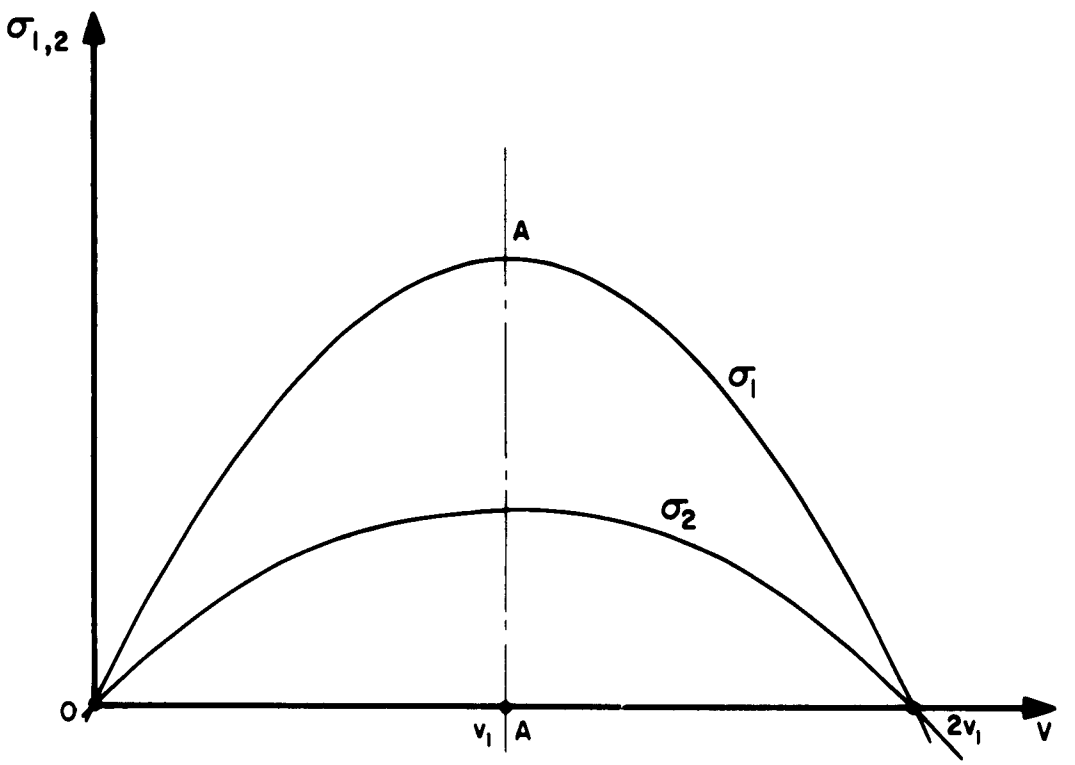

FIG.8 SYMMETRIC VARIATION OF MEMBRANE STRESSES WITH DEFLECTION.

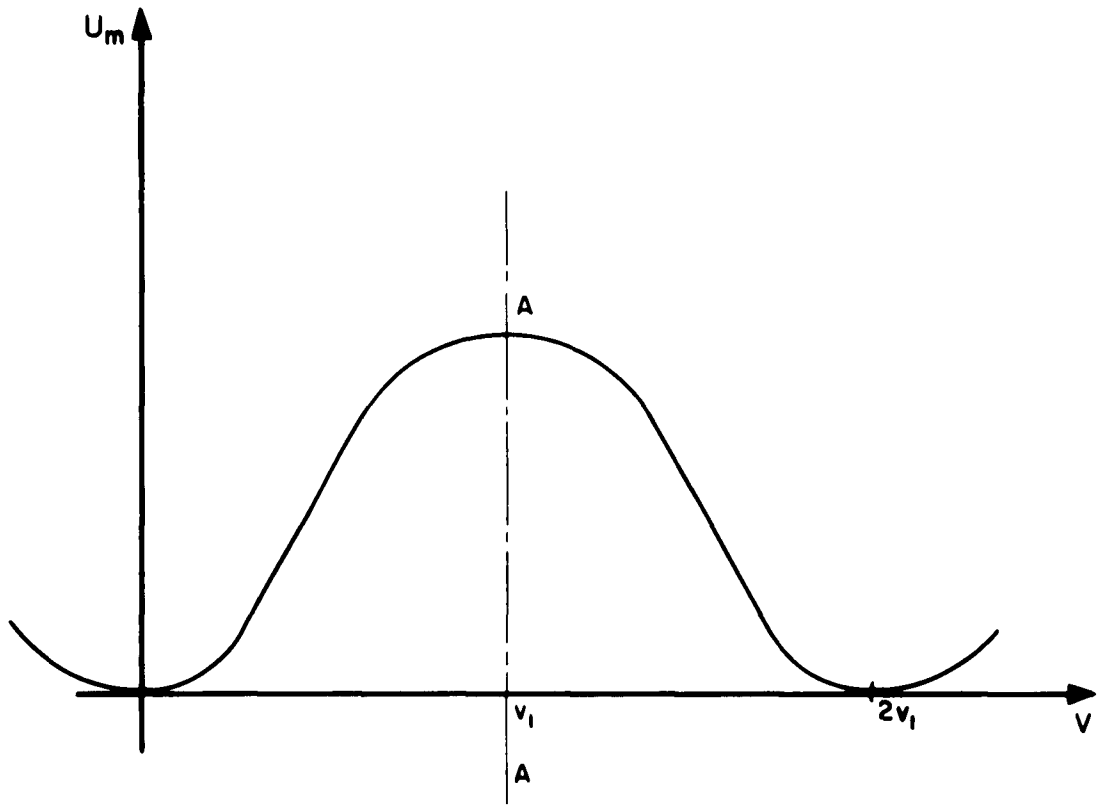

FIG.9 MEMBRANE STRAIN ENERGY VARIATION FOR SYSTEMS SHOWING MEMBRANE STRESS SYMMETRY.

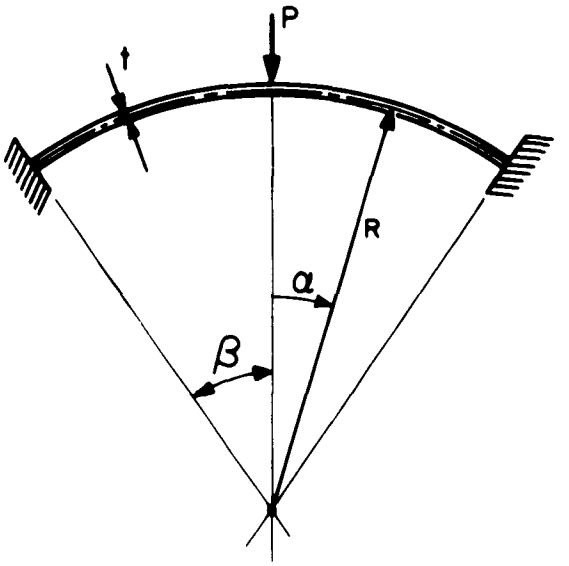

FIG. 10 CLAMPED CIRCULAR ARCH UNDER CENTRAL CONCENTRATED LOAD.

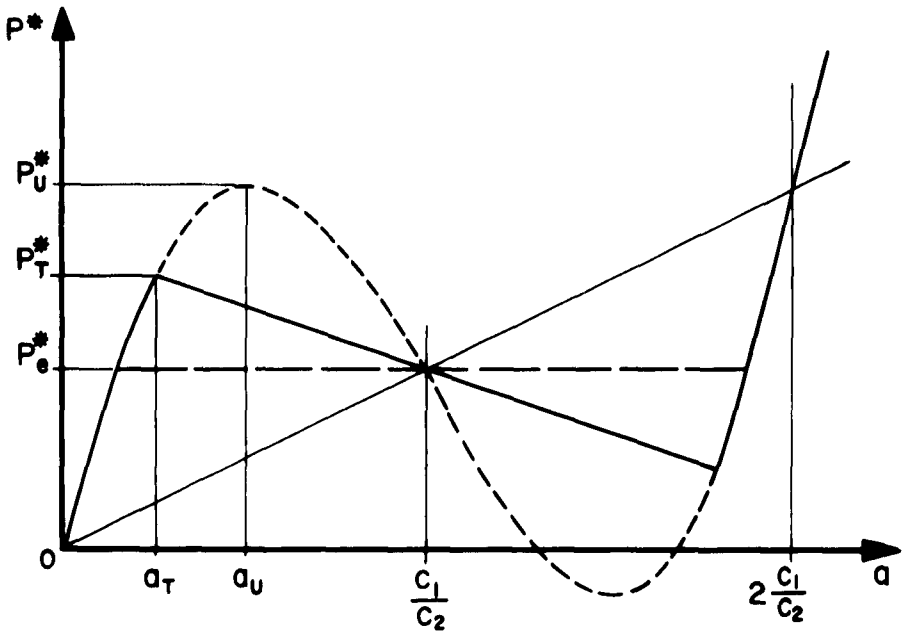

FIG. 11 LOAD DEFLECTION CURVE FOR ARCH SHOWING ANTI-SYMMETRICAL TRANSITIONAL MODE.

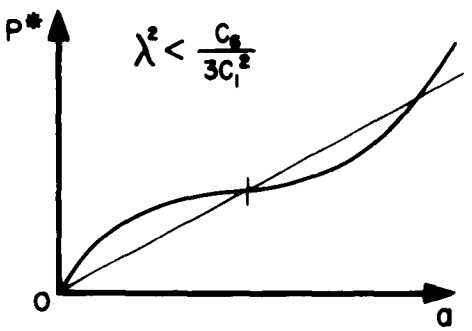

NO BUCKLING

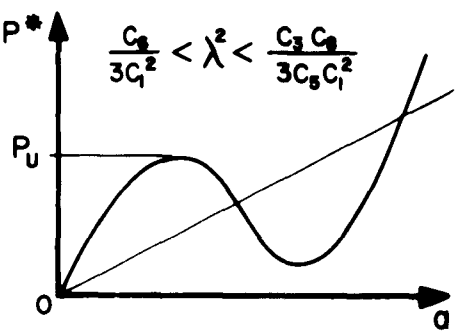

SYMMETRICAL BUCKLING

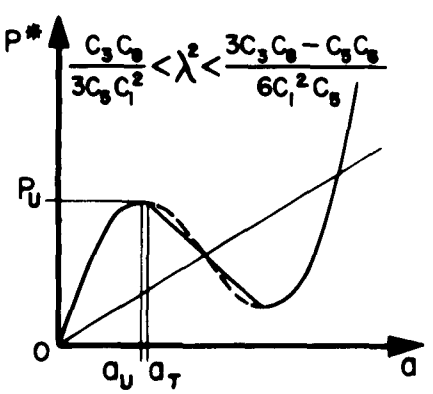

SYMMETRICAL BUCKLING, WITH TRANSITIONAL MODE PRESENT IN UNSTABLE REGION

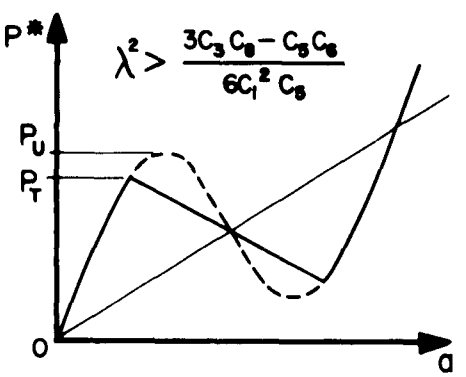

TRANSITIONAL ANTI-SYMMETRICAL BUCKLING

FIG. 12 VARIATION OF BUCKLING MODES WITH λ ($\lambda = \frac{\beta^2 R}{t}$)

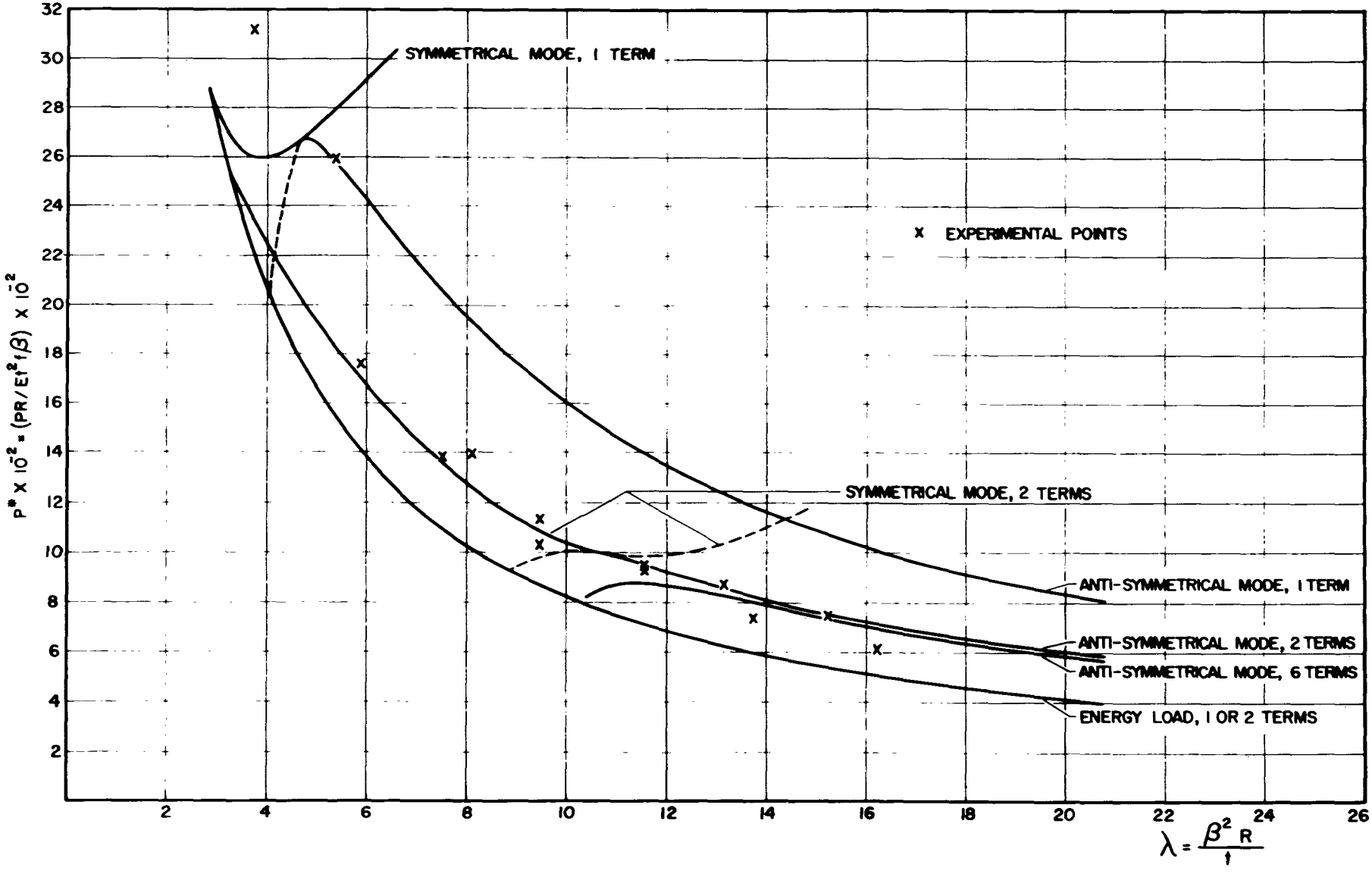

FIG. 13 THEORETICAL AND EXPERIMENTAL BUCKLING VALUES FOR CLAMPED ARCH SUBJECTED TO CENTRAL LOAD

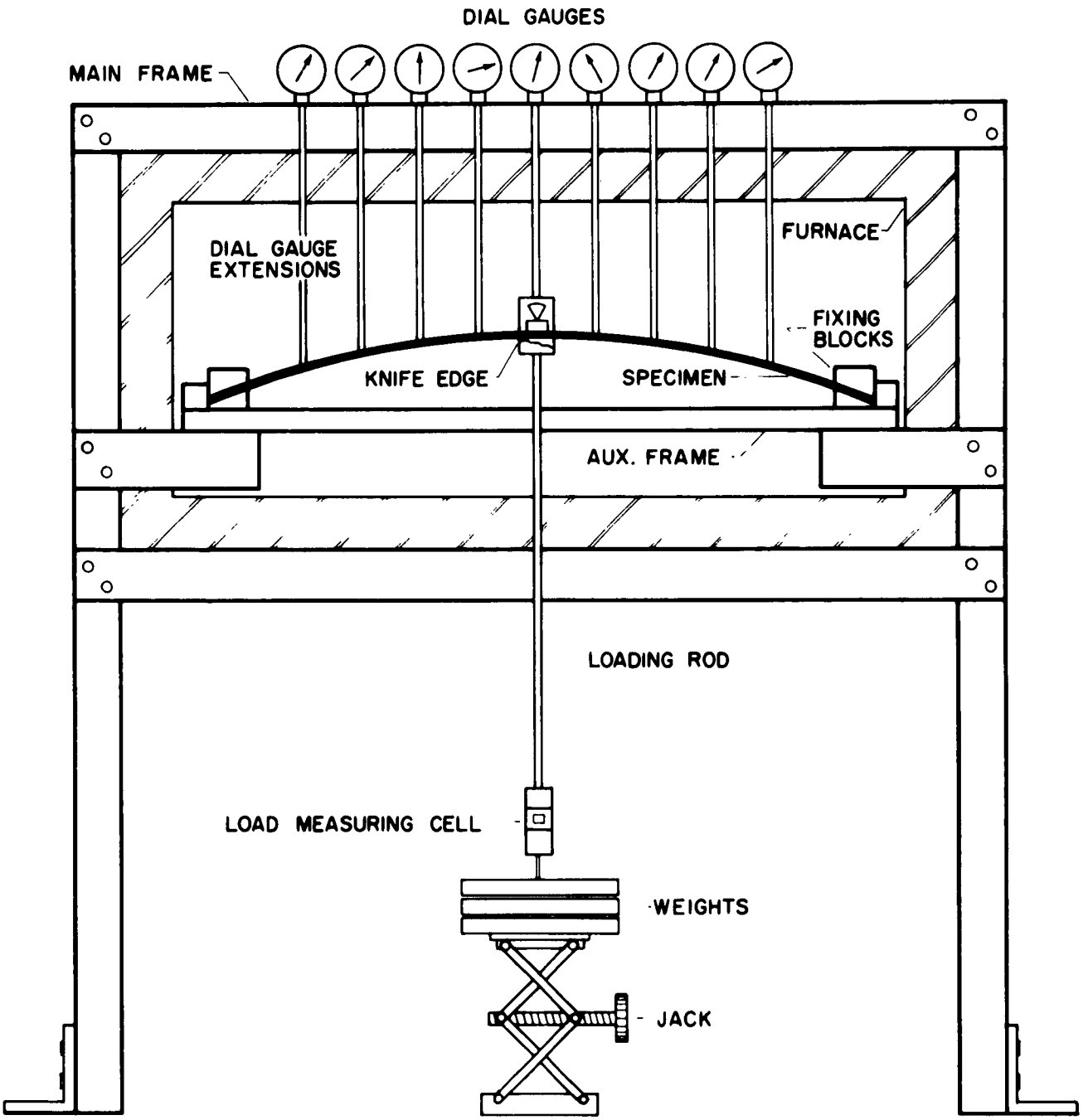

FIG. 14 ELASTIC AND CREEP BUCKLING APPARATUS.

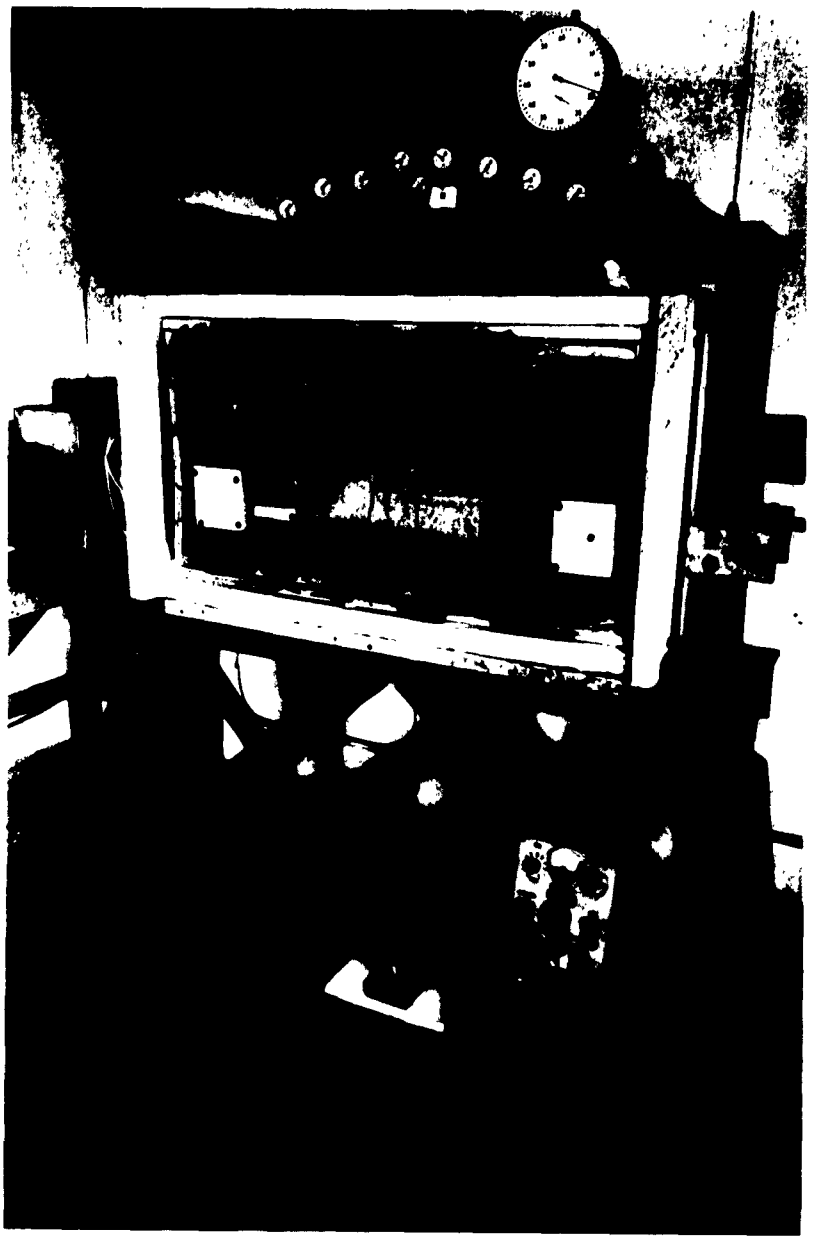

FIG. 15 APPARATUS FOR ELASTIC AND CREEP BUCKLING TESTS OF ARCHES.

FIG. 16 INSIDE OF OVEN SHOWING AUXILIARY FRAME AND LOADED SPECIMEN.

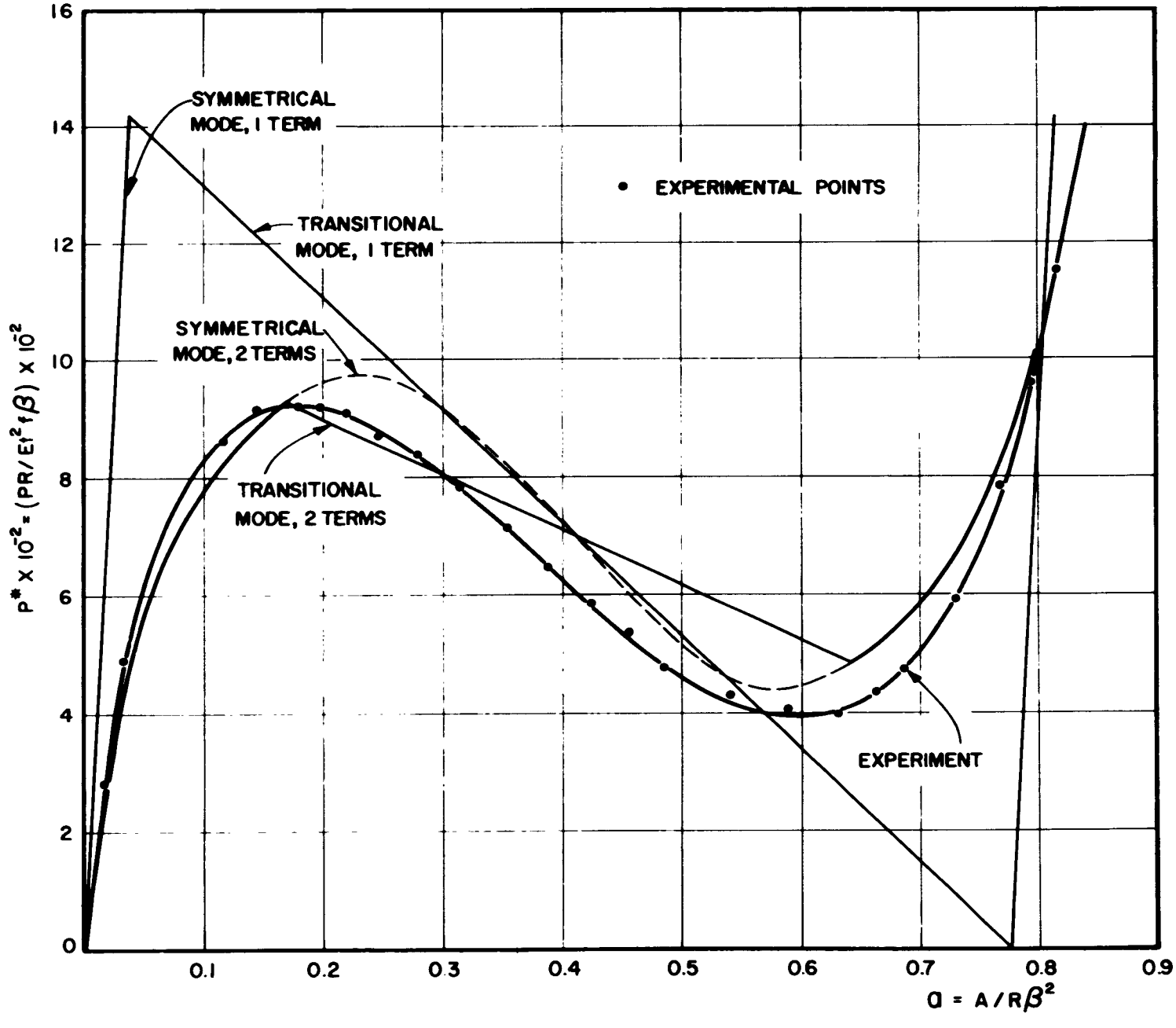

FIG. 17,A LOAD DEFLECTION CURVES FOR THEORY AND EXPERIMENT, $\lambda = 11.62$

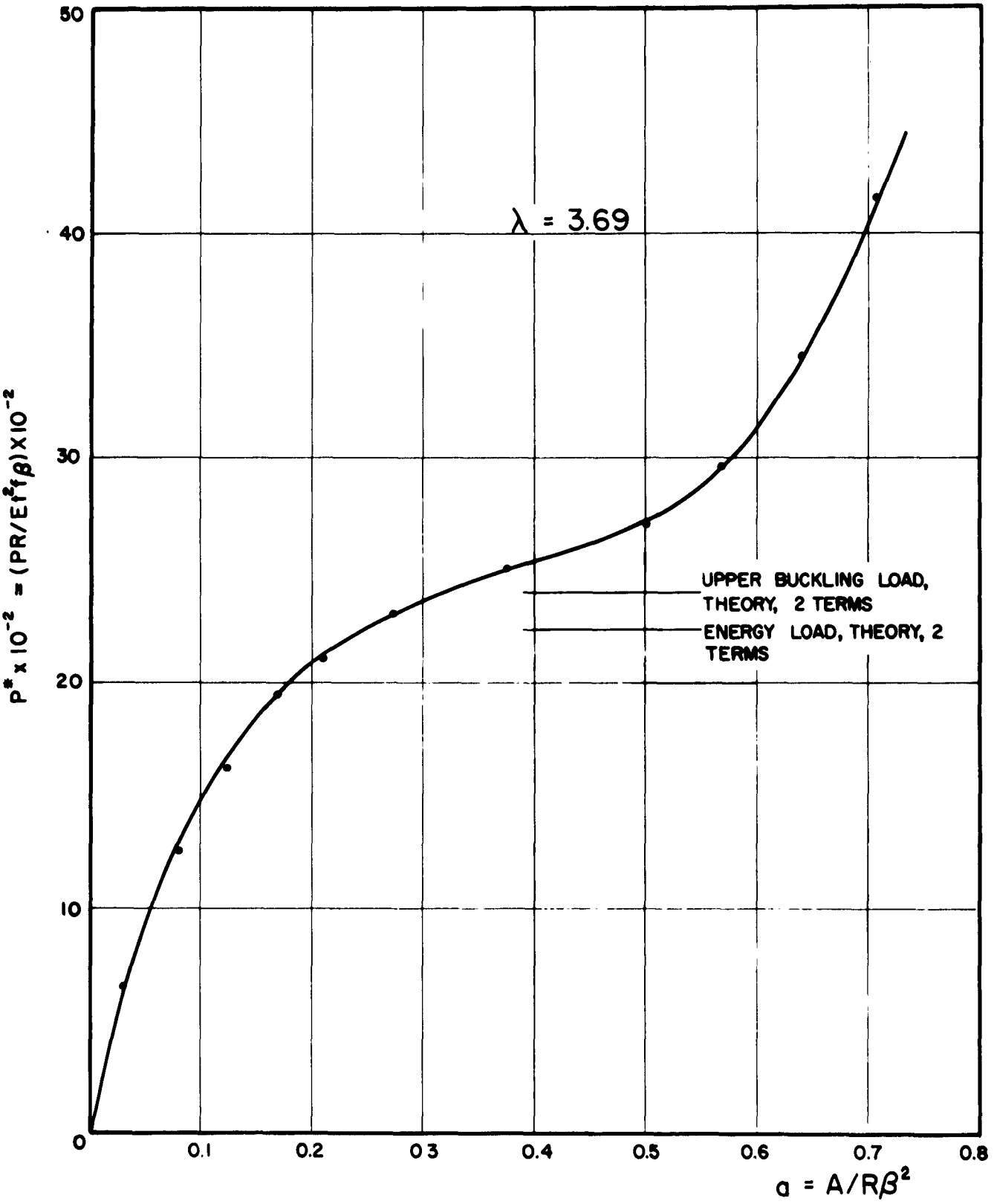

FIG. 17 B EXPERIMENTAL LOAD DEFLECTION CURVE

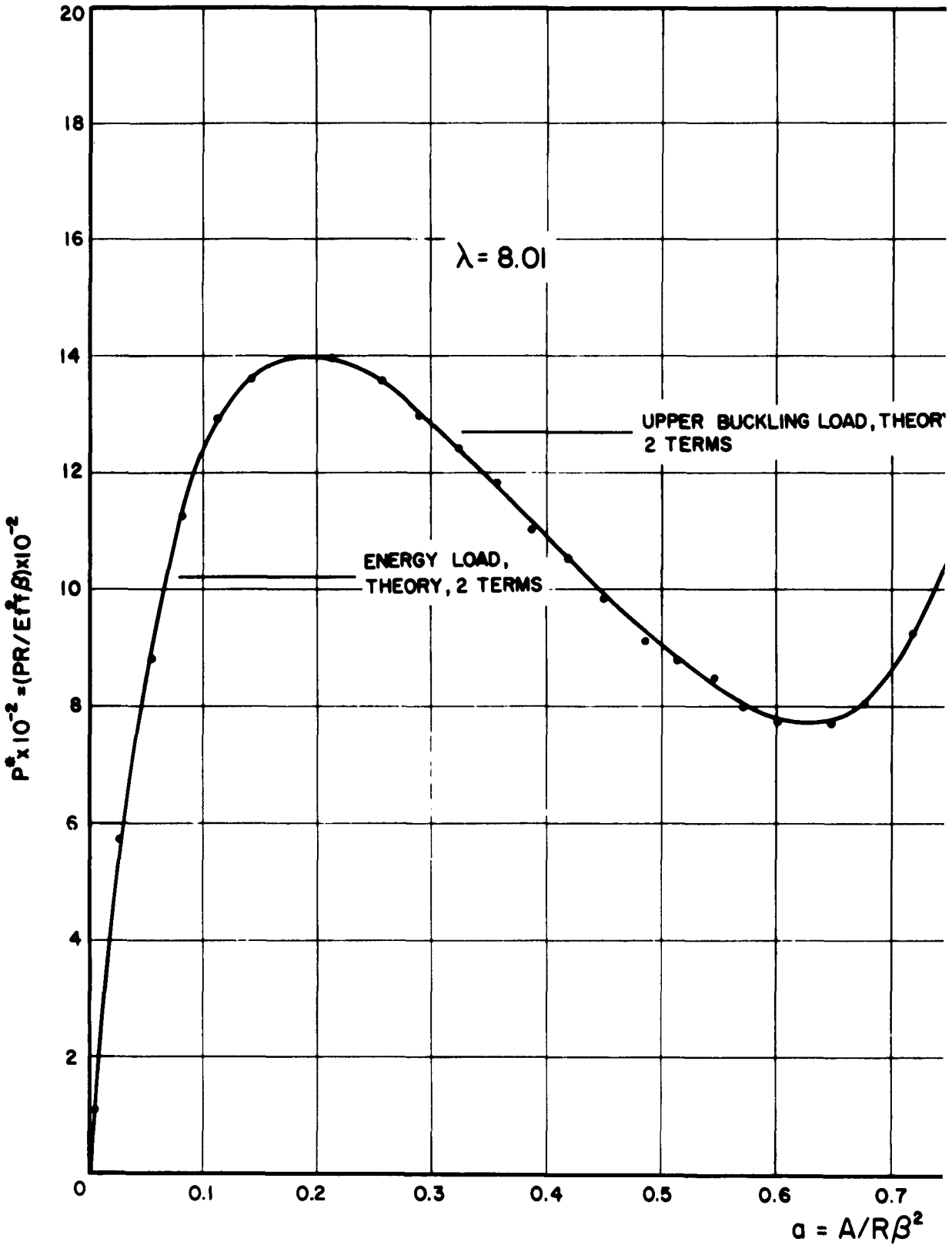

FIG. 17 C EXPERIMENTAL LOAD DEFLECTION CURVE

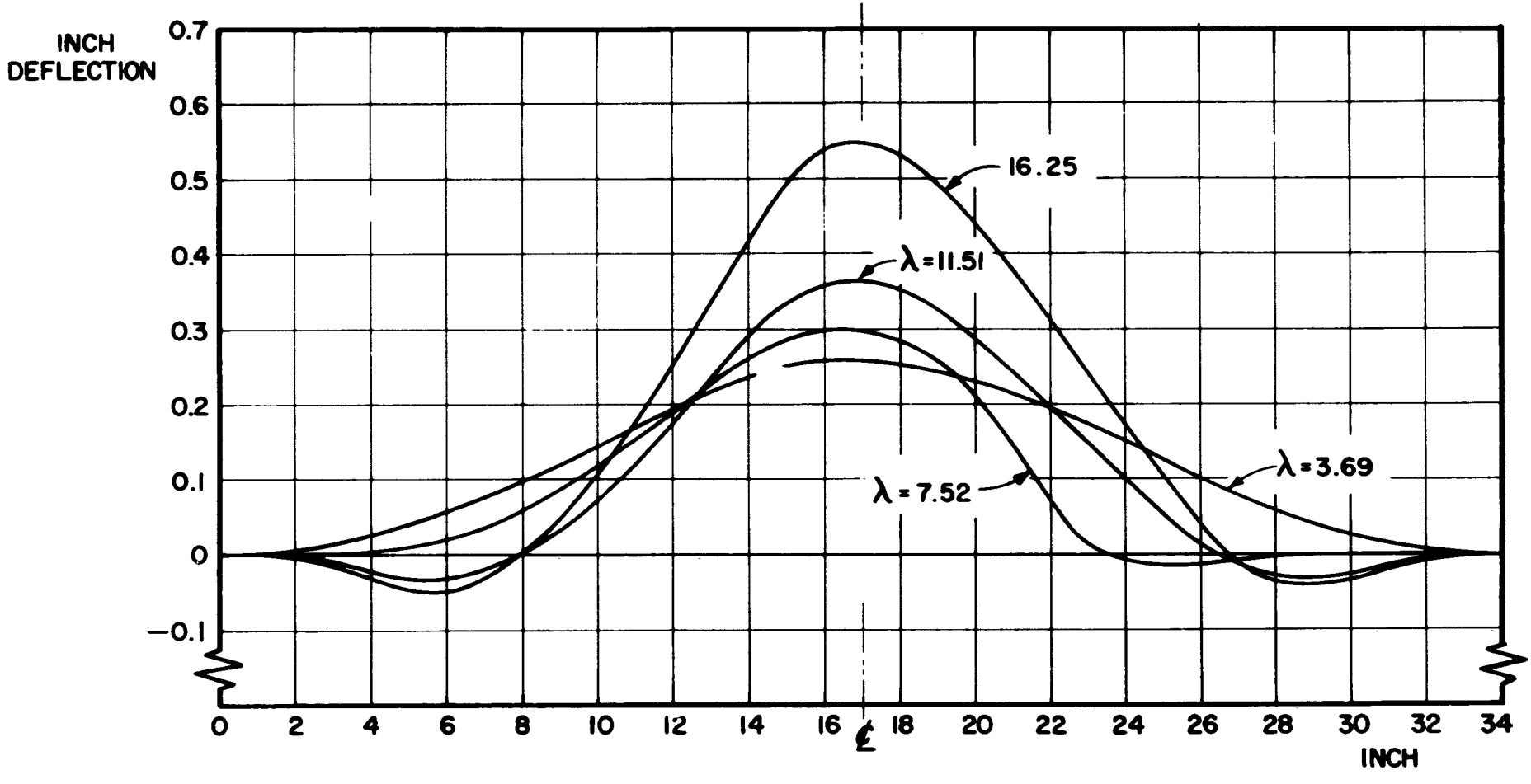

FIG. 18 DEFLECTED SHAPE AT THE BUCKLING LOAD.

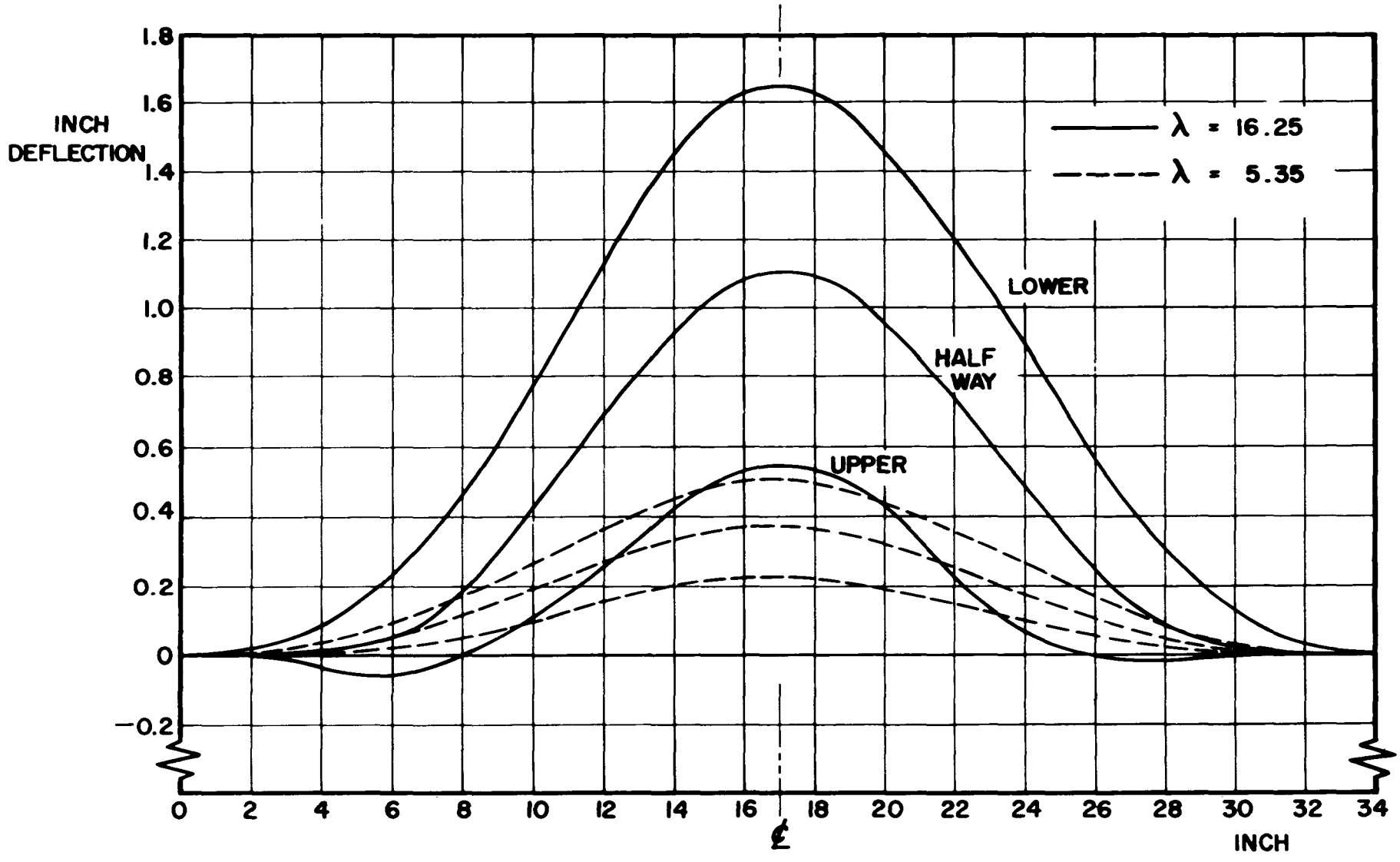

FIG. 19 DEFLECTED SHAPE AT THE UPPER AND LOWER BUCKLING LOAD, AND AT THE MID-POSITION.

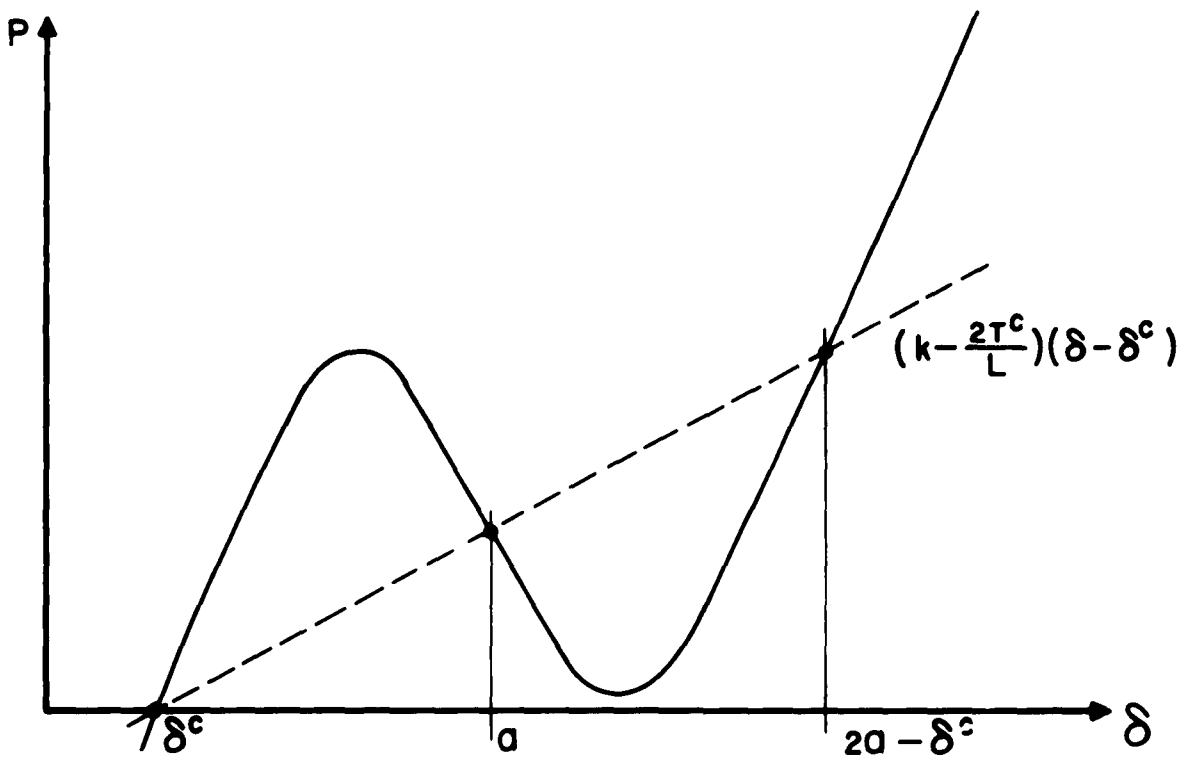

FIG.20 LOAD DEFLECTION RELATION FOR ELASTIC LOADING BEYOND AN INITIAL STRESS STATE.

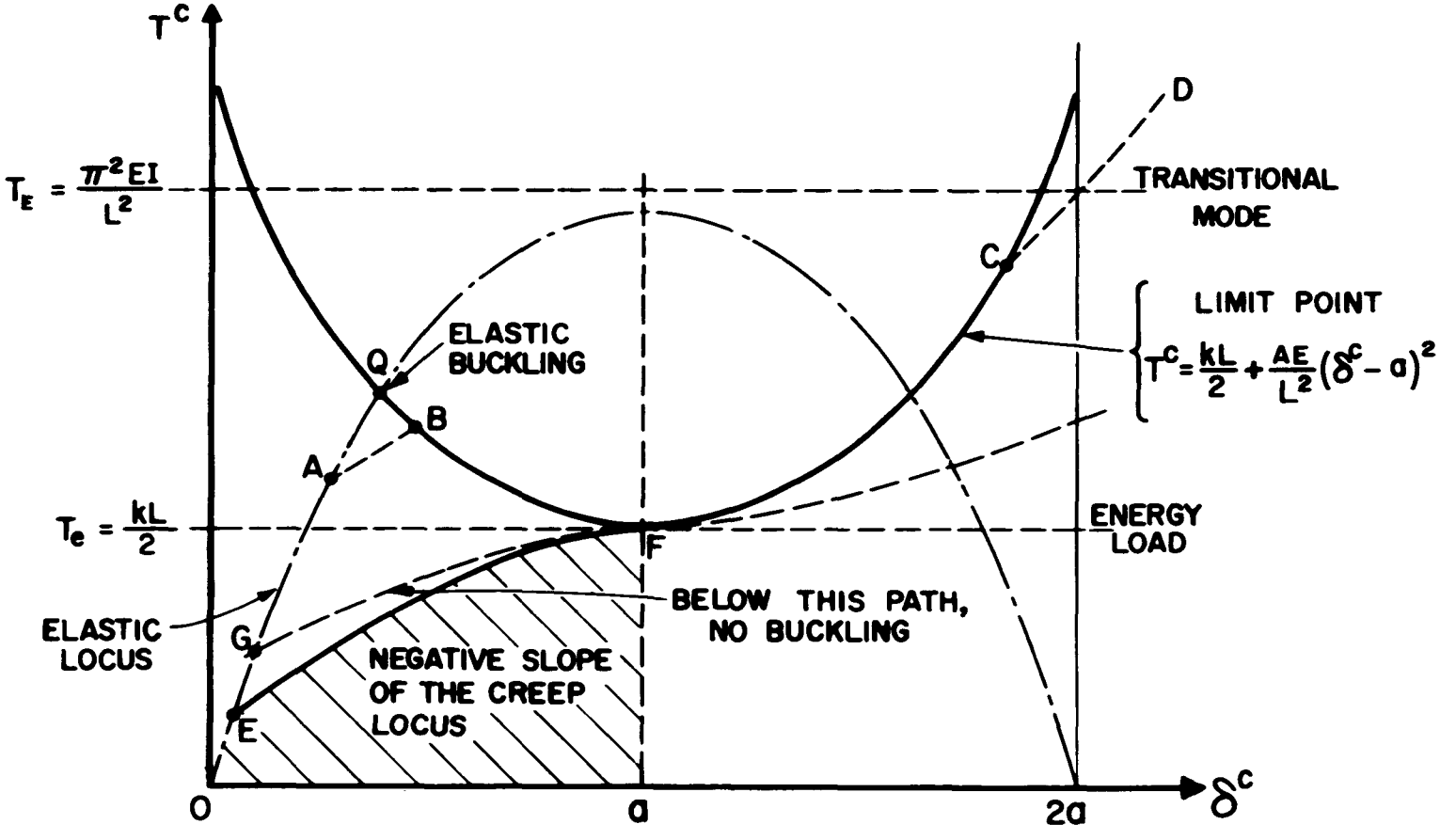

FIG. 21 RELATIONS BETWEEN FORCES IN THE ARMS AND DEFLECTION.

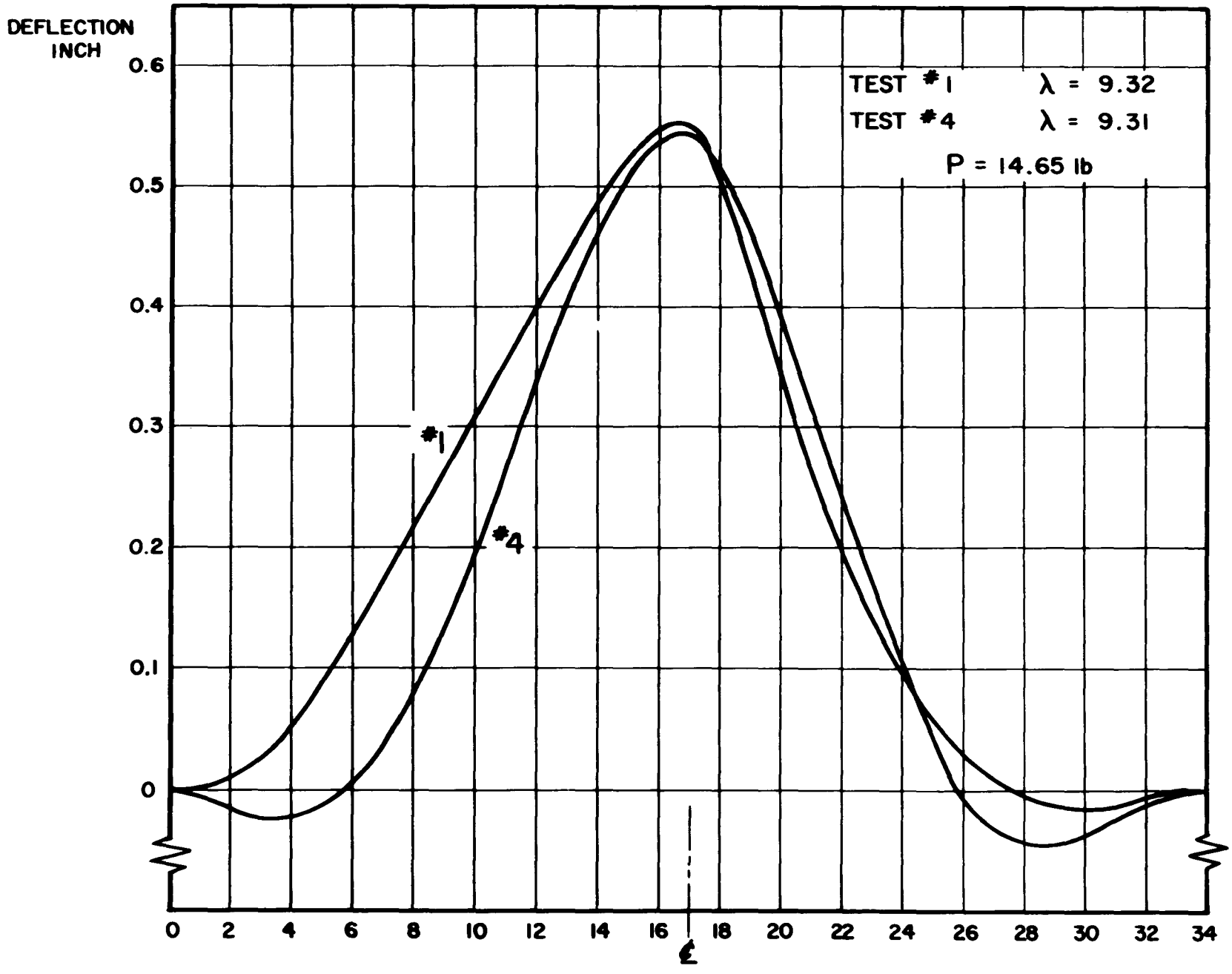

FIG. 22 DEFLECTION JUST PRIOR TO BUCKLING.

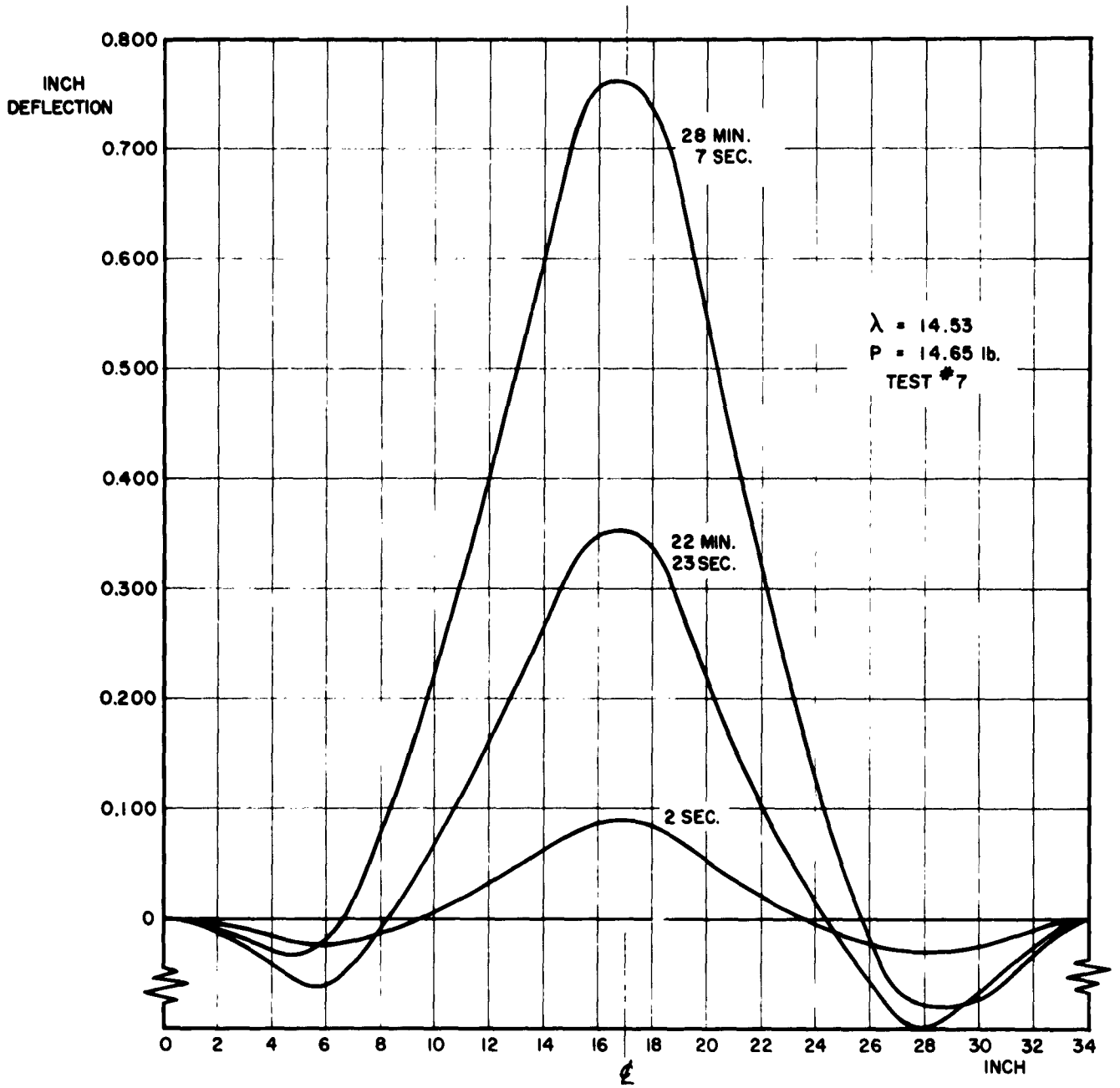

FIG. 23 CHANGE OF DISPLACEMENT WITH TIME.

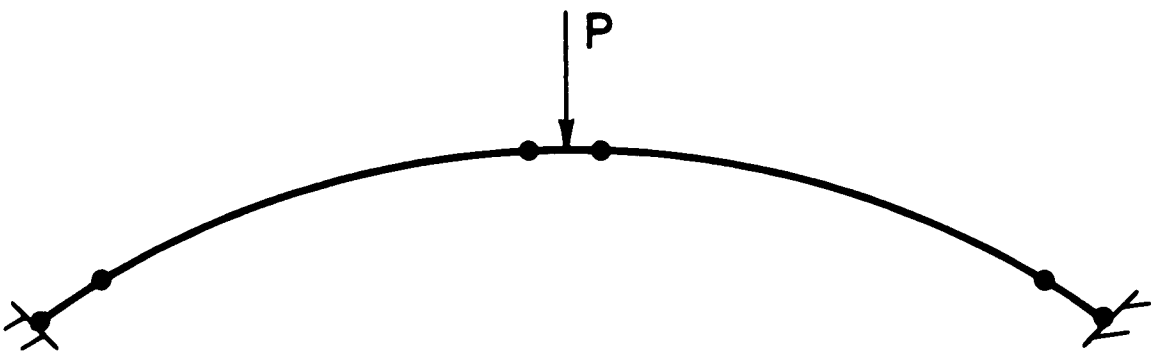

● ELASTIC CREEP HINGES

FIG. 24 SIMPLIFIED ARCH.

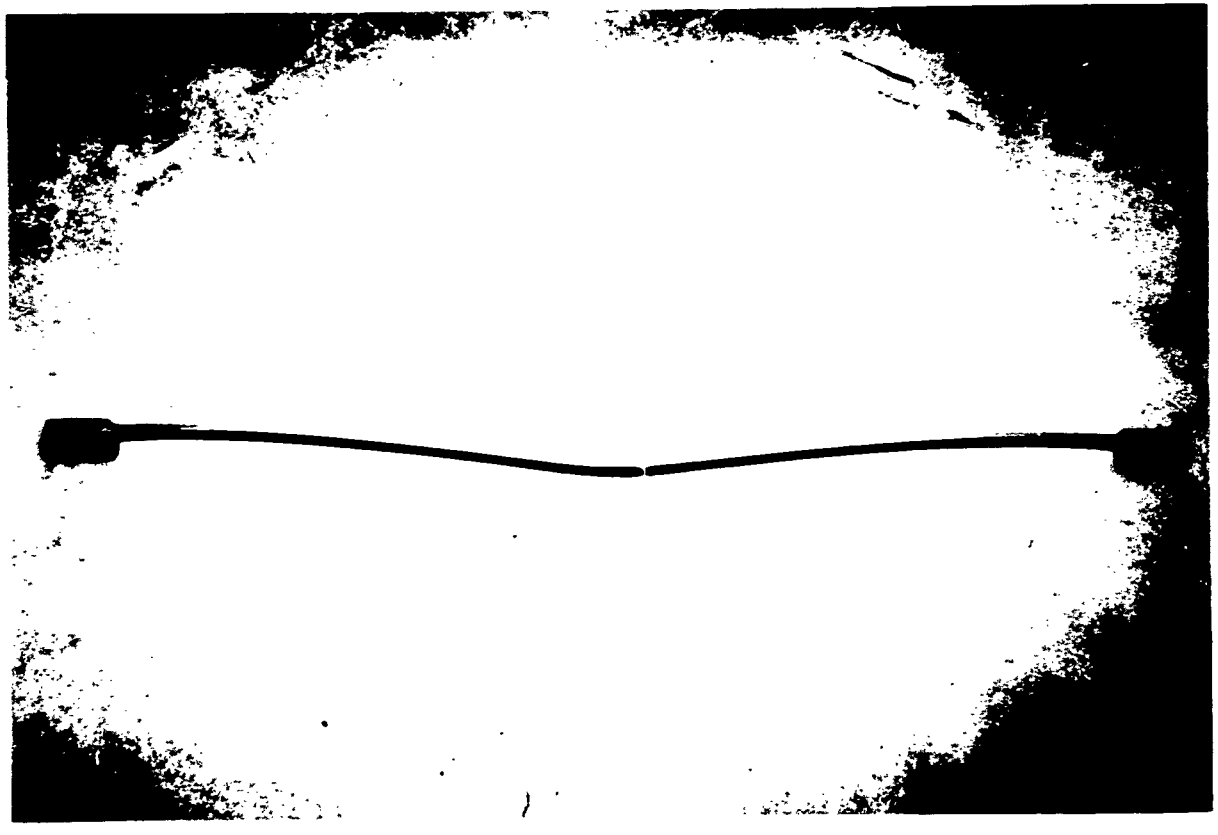

FIG. 25 BUCKLED CREEP SPECIMEN NO. 5 AND FIXING BLOCKS SHOWING SHARP CURVATURE CHANGES AT THE CENTER AND THE ENDS.

DISTRIBUTION LIST FOR UNCLASSIFIED
TECHNICAL REPORTS ISSUED UNDER
Contract Nonr-562(20), Task Nr 064-424

Chief of Naval Research
Department of the Navy
Washington 25, D.C.
Attn: Code 438 (2)
Code 463 (1)

Commanding Officer
Officer of Naval Research
Branch Office
495 Summer Street
Boston 10, Massachusetts (1)

Commanding Officer
Office of Naval Research
Branch Office
John Crerar Library Building
86 E. Randolph Street
Chicago 11, Illinois (1)

Commandin Officer
Office of Naval Research
Branch Office
346 Broadway
New York 13, New York (1)

Commanding Officer
Office of Naval Research
Branch Office
1030 E. Green Street
Pasadena, California (1)

Commanding Officer
Office of Naval Research
Branch Office
1000 Geary Street
San Francisco, California (1)

Commanding Officer
Office of Naval Research
Navy #100, Fleet Post Office
New York, New York (25)

Director
Naval Research Laboratory
Washington 25, D.C.
Attn: Tech. Info. Officer (6)
Code 6200 (1)
Code 6205 (1)
Code 6250 (1)
Code 6260 (1)

Armed Services Technical
Information Agency
ATTN: TIPCR
Arlington Hall Station
Arlington 12, Virginia (10)

Office of Technical Services
Department of Commerce
Washington 25, D.C. (1)

Office of the Secretary of
Defense
Research and Development Division
The Pentagon
Washington 25, D.C.
Attn: Technical Library (1)

Chief
Armed Forces Special Weapons
Project
The Pentagon
Washington 25, D.C.
Attn: Technical Information
Division (2)
Weapons Effects Div. (1)
Special Field Projects (1)
Blast and Shock Branch (1)

Office of the Secretary of
the Army
The Pentagon
Washington 25, D.C.
Attn: Army Library (1)

Chief of Staff
Department of the Army
Washington 25, D.C.
Attn: Development Branch
Res. and Dev. Division (1)
Research Branch
Res. and Dev. Division (1)
Special Weapons Branch
Res. and Dev. Division (1)

Commanding Officer
Engineer Research Development
Laboratory
Fort Belvoir, Virginia (1)

Office of the Chief of Ordnance
Department of the Army
Washington 25, D.C.
Attn: Research and Materials Branch
(Ord. Res. and Dev. Div.) (1)

Office of the Chief of Engineers
Department of the Army
Washington 25, D.C.
Attn: ENG-HL Lib. Br., Adm. Ser. Div. (1)
ENG-WE Eng. Div., Civil Works (1)
ENG-EB Prot. Constr. Br., Eng. Div., Mil. Constr. (1)
ENG-WD Planning Div. Civil Works (1)
ENG-EA Struc. Br., Eng. Div., Mil. Constr. (1)
ENG-NB Special Engr. Br., Eng. Res. and Dev. Division (1)

Office of the Chief Signal Officer
Department of the Army
Washington 25, D.C.
Attn: Engineering and Technical Division (1)

Commanding Officer
Watertown Arsenal
Watertown, Massachusetts
Attn: Laboratory Division (1)

Commanding Officer
Frankford Arsenal
Bridesburg Station
Philadelphia 37, Pennsylvania
Attn: Laboratory Division (1)

Office of Ordnance Research
2127 Myrtle Drive
Duke Station
Durham, North Carolina
Attn: Division of Engineering Sciences (1)

Commanding Officer
Squier Signal Laboratory
Fort Monmouth, New Jersey
Attn: Components and Materials Branch (1)

Chief of Naval Operations
Department of the Navy
Washington 25, D.C.
Attn: Op 37 (1)

Commandant, Marine Corps
Headquarters, U.S. Marine Corps.
Washington 25, D.C. (1)

Chief, Bureau of Ships
Department of the Navy
Washington 25, D.C.
Attn: Code 312 (2)
Code 376 (1)
Code 377 (1)
Code 420 (1)
Code 423 (2)
Code 442 (2)

Chief, Bureau of Aeronautics
Department of the Navy
Washington 25, D.C.
Attn: AE-4 (1)
AV-34 (1)
AD (1)
AD-2 (1)
TD-42 (1)
RS-7 (1)
RS-8 (1)

Chief, Bureau of Ordnance
Department of the Navy
Washington 25, D.C.
Attn: Ad3 (1)
Re (1)
Res (1)
Reu (1)
ReS5 (1)
ReS1 (1)
Ren (1)

Chief, Bureau of Yards and Docks
Department of the Navy
Washington 25, D.C.
Attn: Code D-202 (1)
Code D-202.3 (1)
Code D-220 (1)
Code D-222 (1)
Code D-410C (1)
Code D-440 (1)
Code D-500 (1)

Commanding Officer and Director
David Taylor Model Basin
Washington 7, D.C.
Attn: Code 140 (1)
Code 600 (1)
Code 700 (1)
Code 720 (1)
Code 725 (1)
Code 731 (1)
Code 740 (1)

Commander
U. S. Naval Ordnance Laboratory
White Oak, Maryland
Attn: Technical Library (2)
Technical Evaluation Department (1)

Director
Materials Laboratory
New York Naval Shipyard
Brooklyn 1, New York (1)

Commanding Officer and Director
U. S. Naval Electronics Laboratory
San Diego 52, California (1)

Officer-in-Charge
Naval Civil Engineering Research and Evaluation Laboratory
U. S. Naval Construction Battalion Center
Port Hueneme, California (2)

Director
Naval Air Experimental Station
Naval Air Material Center
Naval Base
Philadelphia 12, Pennsylvania
Attn: Materials Laboratory (1)
Structures Laboratory (1)

Officer-in-Charge
Underwater Explosion Research Division
Norfolk Naval Shipyard
Portsmouth, Virginia
Attn: Dr. A. H. Keil (2)

Commander
U. S. Naval Proving Grounds
Dahlgren, Virginia (1)

Superintendent
Naval Gun Factory
Washington 25, D.C. (1)

Commander
Naval Ordnance Test Station
Inyokern, China Lake, California
Attn: Physics Division (1)
Mechanics Branch (1)

Commanding Officer and Director
Naval Engineering Experimental Station
Annapolis, Maryland (1)

Commanding Officer
USNNOEU
Kirtland Air Force Base
Albuquerque, New Mexico
Attn: Code 20
(Dr. J. N. Brennen) (1)

Superintendent
Naval Post Graduate School
Monterey, California (1)

Commandant
Marine Corps School
Quantico, Virginia
Attn: Director, Marine Corps Development Center (1)

Commanding General
U. S. Air Force
Washington 25, D.C.
Attn: Research and Development Division (1)

Commander
Air Material Command
Wright-Patterson Air Force Base
Dayton, Ohio
Attn: MCREX-B (1)
Structures Division (1)

Commander
U. S. Air Force Institute of Technology
Wright-Patterson Air Force Base
Dayton, Ohio
Attn: Chief, Applied Mechanics Group (1)

Director of Intelligence
Headquarters, U. S. Air Force
Washington 25, D.C.
Attn: P. V. Branch
(Air Targets Division) (1)

Commander
Air Force Office of Scientific Research
Washington 25, D.C.
Attn: Mechanics Division (1)

U. S. Atomic Energy Commission
Washington 25, D.C.
Attn: Director of Research (2)

Director
National Bureau of Standards
Washington 25, D.C.
Attn: Division of Mechanics (1)
Engineering Mechanics Section (1)
Aircraft Structures (1)

Commandant
U.S. Coast Guard
1300 E. Street, N. W.
Washington 25, D.C.
Attn: Chief, Testing and Development Division (1)

U. S. Maritime Administration
General Administration Office Building
Washington 25, D.C.
Attn: Chief, Division of Preliminary Design (1)

National Aeronautics and Space Administration
1515 H Street, N. W.
Washington 25, D.C.
Attn: Loads and Structures Division (2)

Director
Langley Aeronautical Laboratory
Langley Field, Virginia
Attn: Structures Division (2)

Director
Forest Products Laboratory
Madison, Wisconsin (1)

Civil Aeronautics Administration
Department of Commerce
Washington 25, D.C.
Attn: Chief, Aircraft Engineering Division (1)
Chief, Airframe and Equipment Branch (1)

National Sciences Foundation
1951 Constitution Avenue, N.W.
Washington, D.C.
Attn: Engineering Sciences Division (1)

National Academy of Sciences
2101 Constitution Avenue
Washington 25, D.C.
Attn: Technical Director, Committee on Ships Structural Design (1)
Executive Secretary, Committee on Undersea Warfare (1)

Professor Lynn S. Beedle
Fritz Engineering Laboratory
Lehigh University
Bethlehem, Pennsylvania (1)

Professor R. L. Bisplinghoff
Dept. of Aeronautical Engineering
Massachusetts Institute of Technology
Cambridge 39, Massachusetts (1)

Professor H. H. Bleich
Department of Civil Engineering
Columbia University
New York 27, New York (1)

Professor B. A. Boley
Department of Civil Engineering
Columbia University
New York 27, New York (1)

Professor G. F. Carrier
Pierce Hall
Harvard University
Cambridge 38, Massachusetts (1)

Professor Herbert Deresiewicz
Dept. of Mechanical Engineering
Columbia University
632 W. 125th Street
New York 27, New York (1)

Professor D. C. Drucker
Division of Engineering
Brown University
Providence 12, Rhode Island (1)

Professor A. C. Eringen
Division of Engineering Sciences
Purdue University
Lafayette, Indiana (1)

Professor W. Flügge
Dept. of Aeronautical Engineering
Stanford University
Stanford, California (1)

Professor J. N. Goodier
Dept. of Engineering Mechanics
Stanford University
Stanford, California (1)

Professor L. E. Goodman
Engineering Experiment Station
University of Minnesota
Minneapolis, Minnesota (1)

Professor M. Hetenyi
The Technological Institute
Northwestern University
Evanston, Illinois (1)

Professor P. G. Hodge
Department of Mechanics
Illinois Institute of Technology
Chicago 16, Illinois (1)

Professor N. J. Hoff
Dept. of Aeronautical Engineering
Stanford University
Stanford, California (1)

Professor W. H. Hoppmann, II
Department of Mechanics
Rensselaer Polytechnic Institute
Troy, New York (1)

Professor Bruce G. Johnston
University of Michigan
Ann Arbor, Michigan (1)

Professor J. Kempner
Dept. of Aeronautical Engineering
and Applied Mechanics
Polytechnic Institute of Brooklyn
99 Livingston Street
Brooklyn 2, New York (1)

Professor H. L. Langhaar
Dept. of Theoretical and
Applied Mechanics
University of Illinois
Urbana, Illinois (1)

Professor B. J. Lazan, Director
Engineering Experiment Station
University of Minnesota
Minneapolis 14, Minnesota (1)

Professor E. H. Lee
Division of Applied Mathematics
Brown University
Providence 12, Rhode Island (1)

Professor Paul Lieber
Geology Department
University of California
Berkeley 4, California (1)

Professor Hsu Lo
School of Engineering
Purdue University
Lafayette, Indiana (1)

Professor R. D. Mindlin
Department of Civil Engineering
Columbia University
632 W. 125th Street
New York 27, New York (1)

Dr. A. Nadai
136 Cherry Valley Road
Pittsburgh 21, Pennsylvania (1)

Professor Paul M. Naghdi
Mech. Engin., Mechanics & Design
University of California
Berkeley 4, California (1)

Professor William A. Nash
Dept.of Engineering Mechanics
University of Florida
Gainesville, Florida (1)

Professor N. M. Newmark, Head
Department of Civil Engineering
University of Illinois
Urbana, Illinois (1)

Professor Aris Phillips
Department of Civil Engineering
15 Prospect Street
Yale University
New Haven, Connecticut (1)

Professor W. Prager
Computing Center
Brown University
Providence 12, Rhode Island (1)

Professor E. Reissner
Department of Mathematics
Massachusetts Institute of
Technology
Cambridge 39, Massachusetts (1)

Professor M. A. Sadowsky
Department of Mechanics
Rensselaer Polytechnic Institute
Troy, New York (1)

Professor J. Stallmeyer
Department of Civil Engineering
University of Illinois
Urbana, Illinois (1)

Professor Eli Sternberg
Division of Applied Mathematics
Brown University
Providence 12, Rhode Island (1)

Professor S. P. Timoshenko
School of Engineering
Stanford University
Stanford, California (1)

Professor A. S. Velestos
Department of Civil Engineering
University of Illinois
Urbana, Illinois (1)

Professor Enrico Volterra
Dept. of Engineering Mechanics
University of Texas
Austin, Texas (1)

Professor Dana Young
Yale University
New Haven, Connecticut (1)

Professor Bernard W. Shaffer
Dept. of Mechanical Engineering
New York University
New York 53, New York (1)

Dr. John F. Brahtz
Southern California Laboratories
Stanford Research Institute
820 Mission Street (1)
South Pasadena, California

Mr. Martin Goland, President
Southwest Research Institute
8500 Culebra Road
San Antonio, Texas (1)

Mr. S. Levy
General Electric Research
Laboratory
6901 Elmwood Avenue
Philadelphia 42, Pennsylvania (1)

Professor B. Budiansky
Dept. of Mechanical Engineering
School of Applied Sciences
Harvard University
Cambridge 38, Massachusetts (1)

Professor George Herrmann
Department of Civil Engineering
Columbia University
New York 27, New York (1)

Professor E. Orowan
Dept. of Mechanical Engineering
Massachusetts Institute of Technology
Cambridge 39, Massachusetts (1)

Professor J. Ericksen
Mechanical Engineering Department
Johns Hopkins University
Baltimore 18, Maryland (1)

Professor T. Y. Thomas
Graduate Institute for Mathematics and Mechanics
Indiana University
Bloomington, Indiana (1)

Professor Joseph Marin, Head
Department of Engineering Mechanics
College of Engineering and Architecture
The Pennsylvania State University
University Park, Pennsylvania (1)

Professor Robert L. Ketter
Department of Civil Engineering
University of Buffalo
Buffalo 14, New York (1)

Professor W. A. Shaw
Department of Mechanical Engineering
Alabama Polytechnic Institute
Auburn, Alabama (1)

Mr. K. H. Koopman, Secretary
Welding Research Council of The Engineering Foundation
29 W 39th Street
New York 18, New York (2)

Professor Walter T. Daniels
School of Engineering and Architecture
Howard University
Washington 1, D.C. (1)

Professor P. S. Symonds, Chairman
Division of Engineering
Brown University
Providence 12, Rhode Island (1)

Professor Nicholas Perrone
Engineering Science Department
Pratt Institute
Brooklyn 5, New York (1)

Commander
Wright Air Development Center
Wright-Patterson Air Force Base
Dayton, Ohio
Attn: Dynamics Branch (1)
Aircraft Laboratory (1)
WCLSY (1)

Dr. Edward Wenk, Jr.
Executive Secretary
Federal Council for Science & Technology
The White House
Washington, D. C. (1)

Dr. H. G. Hopkins
War Office
Armament Research and Development Establishment
Fort Halstead
Sevenoaks, Kent, England (1)

Professor J. E. Cermak
Department of Civil Engineering
Colorado State University
Fort Collins, Colorado (1)

Professor W. J. Hall
Department of Civil Engineering
University of Illinois
Urbana, Illinois (1)

Professor R. Muki
Division of Mechanical Engineering
Keio University
Koganei-shi
Tokyo, Japan (1)